Carbon dioxide removal efficiency of co-applied and co-pyrolyzed feedstocks for enhanced rock weathering and biochar in a sandy soil

Authors: Maria-Elena Vorrath[1]*, Johannes Meyer zu Drewer[2,3,4], Ingrid Smet[5], Cierra Aldrich[1,6], Lennard Stoeck[1,7], Lara Feiertag[1], Sedrik Nauenburg[1], Ivo Neumann[1], Marvin Scherzinger[8], Theresa Siegmund[8], Dirk Eifler[9], Louise Foster[1], Niko Lahajnar[1], Jens Hartmann[1], Susanne Hamburger[10], Liam Adam Bullock[11], Silvia Placitu[12], Ruadhan Magee[12], Remi Rateau[12], Claudia Kammann[10], Mathilde Hagens[13]

[1]Department of Earth System Science, University of Hamburg, Germany

[2]Ithaka Institute for Carbon Strategies, Goldbach, Germany

[3]Agroscope, Zürich, Switzerland

[4]Institute of Sustainable Energy Systems, Offenburg University, Offenburg, Germany

[5]Carbon Drawdown Initiative, Fürth, Germany

[7]Delft University of Technology, Delft, the Netherlands

[8]Hamburg University of Technology, Hamburg, Germany

[9]Chemistry Department of Chemistry, University of Hamburg, Germany

[10]Hochschule Geisenheim University, Department of Applied Ecology

[11]Geological and Mining Institute of Spain, IGME C/Rios Rosas 23, Madrid, 28003, Spain

[12]Silicate Carbon Limited

[13]Soil Chemistry Group, Wageningen University & Research, Wageningen, the Netherlands

Highlights:

- ERW-biochar effects on carbon sinks are non-additive and material-specific
- Co-application improves mineral weathering and reduces DOC losses
- Co-pyrolysis of biomass and mineral feedstocks enhances biochar stability
- Wet-impregnation with magnesium increases biomass C_{org} conversion into biochar

- Co-pyrolysis can either boost or suppress mineral weathering

Abstract

Enhanced rock weathering (ERW) and pyrogenic carbon capture and storage (PyCCS) are promising land-based approaches for carbon dioxide removal (CDR), yet their co-deployment remains poorly understood. This study investigates how co-application of minerals with biochar and co-pyrolysis of biomass with minerals influence mineral weathering, alkalinity production, and carbon sequestration in a sandy soil with low cation exchange capacity (CEC) and low organic carbon (C_{org}) content. We compared concrete, steel slag, basanite, serpentinised peridotite, limestone and biochar as pure and co-applications, and rock-enhanced biochars (RE-biochars) from dry-mixing and wet-impregnation of biomass and consecutive co-pyrolysis. Downflow columns filled with amended sandy soil were incubated for 75 weeks under elevated pCO_2 while monitoring cation fluxes, trace metal release, dissolved organic carbon (DOC), and changes in soil CEC. Wet-impregnation particularly for Mg-rich feedstocks substantially increased altered RE-biochar properties by increasing the pyrolysis carbon yield and biochar stability. Reduced DOC losses and enhanced alkalinity production, attributed to mineral weathering as the geogenic inorganic carbon sink (IC-Sink), were present for co-applications of biochar with basanite, peridotite, and concrete. In contrast, RE-biochars mostly reduced geogenic IC-Sinks for industrial materials, but increased them for peridotite from accelerated Mg^{2+} release from thermally activated serpentine. Cation pool analyses revealed that most cations were leached rather than being retained in exchangeable pools of the soil. Overall, our evaluation of synergies from ERW-biochar combinations clearly highlights material-specific advantages and trade-offs, supporting the recommendation of both single application and co-application of biochar with mineral feedstocks.

Keywords: rock-enhanced biochar, impregnation, RE-biochar, carbon dioxide removal, pyrogenic carbon, biochar stability, climate change mitigation

1 Introduction

Limiting global warming and securing food production increasingly rely on land-based strategies of carbon dioxide removal (CDR) (Shukla et al., 2022; Smith et al., 2024). Agriculture contributed 13-21% of global anthropogenic greenhouse gas emissions between 2010 and 2019, but also offers major potential for durable CDR through soil-based interventions (Babiker et al., 2022; Nabuurs et al., 2022). Enhanced rock weathering (ERW) accelerates mineral dissolution whilst converting atmospheric CO_2 into bicarbonate that can be stored for millennia (Hartmann et al., 2013; Renforth, 2019), while pyrogenic carbon capture and storage (PyCCS) stabilizes biomass carbon through pyrolysis, producing durable biochar (Schmidt et al., 2025, 2019). Together, these methods offer long-term carbon sinks (C-Sinks) and potentially improve agronomic performance (Schmidt et al., 2021; Vorrath et al., 2025), offering valuable opportunities for climate mitigation amid widespread soil degradation and increasing climate-related pressures on agriculture (Mbow et al., 2022; Nabuurs et al., 2022; Shukla et al., 2022).

The performance of ERW and biochar is closely linked to soil health and nutrient cycling, both of which are often impaired in degraded or drought-prone systems. Soil amendments that enhance productivity while strengthening carbon storage could therefore accelerate the adoption of these CDR approaches (Janssens et al., 2022; Waring et al., 2023). Biochar can improve soil fertility, increase nutrient availability, enhance water retention, promote root growth, and increase crop yields, particularly in tropical, highly weathered soils (Lehmann et al., 2021; Schmidt et al., 2021), while also reducing soil nitrate leaching and N_2O emissions (Borchard et al., 2019), immobilizing trace elements (Peng et al., 2018; Schmidt et al., 2021), and supporting soil remediation efforts (Cornelissen et al., 2025; Wang et al., 2022). Enhanced rock weathering can further raise soil pH, supply macro- and micronutrients, and enhance soil structure (Beerling et al., 2018; Dupla et al., 2024; Haque et al., 2020; Swoboda et al., 2022). During weathering, Mg^{2+}- and Ca^{2+}-bearing minerals react with atmospheric CO_2 to form bicarbonate and increase soil alkalinity, enabling its export to aquatic systems and reintroducing carbon into the geological cycle (Hartmann et al., 2013; Renforth, 2019). Further, this process promotes secondary mineral formation in the soil that stabilizes soil organic carbon (SOC) and protects labile biochar fractions (Buss et al., 2023; Yang et al., 2021). These combined agronomic and biogeochemical effects highlight the need to better understand the interactions between ERW and biochar and whether their combined use can

more effectively enhance long-term CDR while supporting resilient and productive agricultural systems.

In addition to Ca^{2+}- and Mg^{2+}-rich silicate and carbonate rocks, industrial by-products such as steel slag or recycled concrete fines are increasingly explored as ERW feedstocks due to their high reactivity, broad availability, and alignment with circular-economy principles (McDermott et al., 2024; Renforth, 2019; Xu et al., 2024). Furthermore, weathering rates of all feedstocks depend on multiple factors, including water availability (Cipolla et al., 2022; Deng et al., 2023), mineral speciation (Heřmanská et al., 2023, 2022), particle size and specific surface area (Rinder and von Hagke, 2021), pCO_2 and soil pH (Amann et al., 2022), temperature (Oelkers et al., 2018; Xu et al., 2024), and soil biota (Niron et al., 2024; Sohng et al., 2025; Vicca et al., 2022). When combined with biochar, which is composed of persistent and semi-persistent carbon fractions (Keiluweit et al., 2010; Schmidt et al., 2022) that undergo gradual biotic and abiotic oxidation in soils after application (Pignatello et al., 2024), these ERW feedstocks may further increase long-term carbon sequestration.

Interest in interactions between ERW and biochar has grown, as co-application may enhance water retention (Li et al., 2021; Sun and Lu, 2014), improve drainage (Vorrath et al., 2025), increase soil pCO_2 through stimulated microbial activity (Palansooriya et al., 2019), increase the soil cation exchange capacity (CEC) (Omara et al., 2023) or promote mineral-associated organic matter (MAOM) formation (Buss et al., 2023; Han et al., 2020). Minerals may also protect biochar from oxidation, thus reducing the decay of organic carbon (C_{org}) in the soil (Nan et al., 2022). However, pot experiments have found only additive or modest synergistic effects on ERW (Honvault et al., 2024; Te Pas et al., 2026). Beyond co-application, recent studies show that adding minerals to biomass before pyrolysis to create rock-enhanced (RE-)biochar has additional benefits (Meyer zu Drewer et al., 2025). Mg^{2+}- and Ca^{2+}-bearing additives can enhance carbon retention, char aromatization, stability, and ash composition (Buss et al., 2019; Grafmüller et al., 2022; Mašek et al., 2019; Nan et al., 2020), while thermal treatment can alter the mineral surface area (Jiang et al., 2022; Mahanta et al., 2016), change mineral speciation of e.g. serpentines (Du Breuil et al., 2019; Kelemen et al., 2011), or passivate reactive surfaces by pyrogenic carbon coatings (Meyer zu Drewer et al., 2025). Although some studies report unchanged pyrogenic carbon yields (Meyer zu Drewer et al., 2025), others find increases after adding wood ash, potassium acetate, or rock powders (Buss et al., 2019; Grafmüller et al., 2022; Mašek et al., 2019).

Despite recent advances, major uncertainties remain regarding the combined use of ERW and biochar because most existing studies examine single materials in isolation, without systematically comparing biochar, minerals, their co-application, and RE-biochars under identical conditions on the same soil. Consequently, it is still unclear whether co-applying biochar and rock powders enhances mineral dissolution, alkalinity export, or long-term CDR beyond the largely additive effects observed so far (Honvault et al., 2024; Te Pas et al., 2026). Additionally, little is known about how co-application influences soil solution chemistry, dynamics of dissolved organic carbon (DOC), microbial processes, or the formation of secondary minerals that could stabilize organic matter or retain cations (Buss et al., 2023). A further unresolved issue is how to distinguish between alkalinity originating from mineral weathering (geogenic) or biomass decomposition (biogenic), as cations from short-term biogenic cycling do not contribute to additional CDR, while geogenic cations released through ERW do (Vorrath et al., 2025). This is essential for accurate CDR accounting and assessing the climate change-mitigation potential of mixed amendments. For co-pyrolysis, central uncertainties for mineral feedstocks include whether thermal treatment accelerates or suppresses weathering through changes in mineral structure, specific surface area, or surface passivation (Mahanta et al., 2016; Meyer zu Drewer et al., 2025). Furthermore, interactions with soil pCO_2, soil biota, trace metal mobility, and organo-mineral associations remain largely untested in controlled soil systems. These uncertainties hinder the development of robust monitoring, reporting and verification (MRV) frameworks and limit the ability to design effective, scalable land-based CDR strategies.

This study examines how co-application and co-pyrolysis of various mineral feedstocks with biochar influence mineral weathering, alkalinity production, and carbon sequestration in a sandy, low-CEC, low-C_{org} soil. Under elevated CO_2 conditions (1-1.2 vol-% CO_2), we compared pure applications of concrete, steel slag, basanite, peridotite, limestone, and biochar, co-applications of biochar with mineral feedstocks, and eight RE-biochars (produced through both dry-mixing and wet-impregnation) in a downflow soil column setup. The four objectives of the study are:

1) to test two mineral-enhancement procedures: adding minerals either as dry rock powder (dry-mixing) or suspended in water (wet-impregnation) to the biomass prior to pyrolysis, and evaluate their impact on C_{org} conversion and carbon stability in RE-biochars;

2) to assess the development of the different C-Sinks from both ERW and PyCCS, cation and trace metal release, and effects on soil organic carbon (SOC) and DOC of all applications during a 75-week incubation experiment;
3) to identify possible synergistic effects of co-application and RE-biochars on mineral weathering and trace metal retention; and
4) to determine the distribution of released cations between soil and leachate.

This work provides the first integrated assessment of combining diverse mineral feedstocks with biomass for a joint CDR approach in soils, with relevance for land-based CDR scalability.

2 Materials and Methods

2.1 Materials and pyrolysis

2.1.1 Feedstocks

As the biomass feedstock a mixture of wood chips from spruce, 0.8-1.1 mm (*Picea abies* L.) and soybean meal, 0-0.5 mm (*Glycine max* L.) was utilized. The high oil content of the latter served as a lubricant in the pelleting process. Mineral feedstocks included industrial materials of 1) returned concrete, 0.5-1020 µm (provided by *Silicate Carbon Limited*), and 2) steel slag, 0.5-720 µm (*BaseLith* provided by *Thyssen Krupp*), and silicate rock of 3) basanite, 0.5-210 µm (*Eifelgold* from *Rheinische Provinzial-Basalt- und Lavawerke GmbH & Co. oHG*) and 4) serpentinised peridotite, 0.5-250 µm (*Dunite No.11* provided by *Sibelco*). Limestone, 0.5-2460 µm, was included as an additional control to compare amendments with the common farming practice of liming. Additional details on the mineral feedstocks are provided in the supplementary information, including grain size distribution (supplementary information S1) and specific surface area (supplementary data D1), mineralogical and chemical composition (supplementary data D2) and the thermogravimetric analysis of concrete and steel slag (supplementary data D3).

2.1.2 Feedstock preparation

Pure biochar was produced from spruce chips and soybean meal in a 50:50 mass ratio. Co-pyrolysis of biomass with minerals (biomass:mineral in a 70:30 mass ratio) was conducted in two ways (Table 1). Feedstocks were either dry-mixed or wet-impregnated. While dry-mixing is a standard preparation approach already described in previous studies (Meyer zu Drewer et al., 2025; Vorrath et al., 2025), wet-impregnation was a novel approach, in which

the biomass was soaked in a mineral suspension produced from the mineral feedstock to introduce dissolved cations into the biomass prior to pyrolysis (Figure 1). The steps were:

1) Suspension of 2100 g mineral feedstock in 2 L deionized water (DI) to produce a cation-enriched suspension. Stirring was facilitated by a Kitchen Aid (45 rpm, room temperature) to promote mineral dissolution and cation release from the minerals.
2) After five days, 4900 g of the spruce-soybean mix was soaked in the mineral suspension while the remaining mineral feedstocks were oven-dried (80 °C) separately.
3) The mixture was then air-dried at 20° C to evaporate the water.
4) The remaining mineral feedstocks was added to the biomass afterwards.

Table 1: Configuration of biochar and rock-enhanced biochars.

No.	ID	Type	Mineral feedstock	Mass ratio biomass:mineral	Processing
1	ConcreteChar-dry	RE-biochar	Concrete	70:30	dry-mixed and co-pyrolyzed
2	ConcreteChar-wet	RE-biochar	Concrete	70:30	wet-impregnated and co-pyrolyzed
3	SteelslagChar-dry	RE-biochar	Steel slag	70:30	dry-mixed and co-pyrolyzed
4	SteelslagChar-wet	RE-biochar	Steel slag	70:30	wet-impregnated and co-pyrolyzed
5	BasaniteChar-dry	RE-biochar	Basanite	70:30	dry-mixed and co-pyrolyzed
6	BasaniteChar-wet	RE-biochar	Basanite	70:30	wet-impregnated and co-pyrolyzed
7	PeridotiteChar-dry	RE-biochar	Peridotite	70:30	dry-mixed and co-pyrolyzed
8	PeridotiteChar-wet	RE-biochar	Peridotite	70:30	wet-impregnated and co-pyrolyzed
9	Biochar	Biochar	none	100:0	pyrolyzed

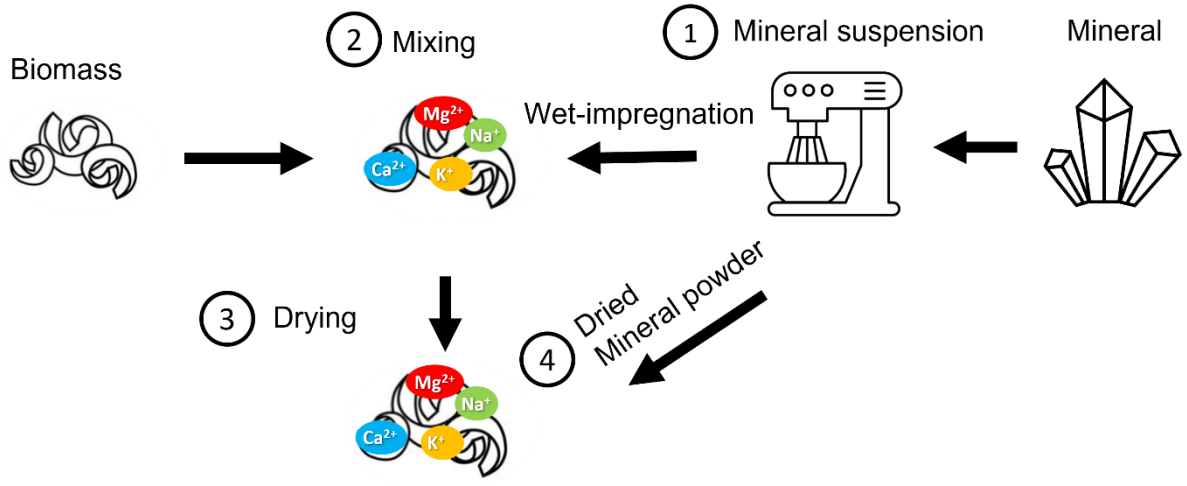

Figure 1: Description of the processing of feedstocks for wet-impregnated RE-biochar. 1) The mineral feedstock is suspended in deionized water for 5 days and 2) the suspension is mixed with the biomass. 3) After air-drying to evaporate the water from the biomass, the 4) remaining oven-dried mineral feedstock is added and mixed in as well.

All feedstock mixtures (dry-mixed and wet-impregnated) were pelleted to 6 mm on an Amandus Kahl pellet press at the Hamburg University of Technology. Prior to pyrolysis, the dry matter content of all feedstock pellets was determined at 105°C. The elemental composition of raw feedstocks was analysed by Eurofins Umwelt-Ost GmbH, Germany (supplementary data D4). Calculations of how much C_{org} converted into biochar (C_{org} conversion) and rock content were conducted following the procedure described in Meyer zu Drewer et al. (2025).

All biochar and RE-biochars were pyrolyzed at 650 °C for approximately 15 min. in a PYREKA pyrolysis unit by *Novocarbo* in Dörth, Germany (details described in supplementary information S2) and their elemental compositions were analysed by Eurofins Umwelt-Ost GmbH, Germany, following the guidelines of the European Biochar Certificate (EBC, 2024). Hydropyrolysis (HyPy) was performed using the approach outlined by Meredith et al. (2017) (see supplementary information S2) to determine the fraction of stable polycyclic aromatic carbon, which contains more than 7 fused aromatic rings that exhibit high environmental stability (Hagemann et al., 2025). This fraction is expressed as BC_{HyPy}, the stable fraction remaining of the initial C_{org} content, and has a high probability to persist for >1000 years in soils, thus being eligible as permanent CDR in the voluntary carbon market (Schmidt et al., 2025).

2.1.3 Soil

The soil utilized in the incubation experiments was sourced from an agricultural field in Gartow, Germany, in March 2023, and had already been analysed by Ansari et al. (2026). The soil is classified as a pure sand with a 93.8% sand fraction, a total carbon content of 1.24% (1.2% C_{org}, 0.04% inorganic carbon, IC) and low CEC of 21.0 mmol kg^{-1} (further details given in supplementary information S3).

2.2 Incubation experiment and analyses

The incubation experiment was designed based on Vorrath et al. (2025) with 25 cm long vertical soil columns. 500 g of sandy soil was mixed with either 10 g of biochar pellets (40.6 t ha^{-1}) and/or 9.9 g of loose mineral feedstocks (40.2 t ha^{-1}) or 15.0-16.3 g of RE-biochar (60.9-66.2 t ha^{-1}) adjusted to contain 9.9 g of mineral feedstock per column. Each combination was installed as duplicates. The experiment was conducted under elevated pCO_2 levels corresponding to 1.0 ± 0.4 vol-% (box 1) and 1.2 ± 0.6 vol.-% (box 2), watered with CO_2 gasified deionized water (equivalent to annual rainfall of 820 mm) over 75 weeks in a dark room at around 22° C. Leachate samples were collected in weeks 2, 4, 6, 9, 15, 19, 27, 39, 51, 63 and

75 (further details described in supplementary information S4). After the experiment, the soil CEC and exchangeable cations were measured on pooled samples from duplicates with the same treatment.

At each sampling event, pH, temperature, and EC were measured immediately upon leachate collection using a WTW 3630 IDS Multimeter. Dissolved inorganic carbon (DIC) was sampled directly inside the incubator to avoid re-equilibration with atmospheric CO_2. Total alkalinity (TA), major ions, dissolved organic carbon (DOC), and dissolved silica (DSi) were subsequently analysed from filtered samples, while trace metals were analysed on pooled leachate samples after weeks 9 and 27 via atomic absorption spectroscopy (all details in supplementary information S5). For the leachate analyses, DIC was determined using a Picarro G2131-I cavity ring-down spectrometer coupled to an AutoMate FX preparation device, TA by automated titration to pH 4.3 with 0.02 N HCl following Dickson (1981), major cation and anions by ion chromatograph, DSi by the molybdate blue calorimetric method, and DOC by high-temperature combustion with non-dispersive infrared detection (supplementary information S5).The parameters DIC, TA, major ions, DOC and DSi were additionally determined on the mineral suspensions (all details in supplementary information S5).

The CEC of soil after the experiment was determined by Qmineral Analysis & Consulting (Belgium) using the ammonium acetate saturation method of Kitsopoulos (1999), and major cations exchanged were quantified by inductively coupled plasma atomic emission spectroscopy (ICP-OES). In carbonate-rich soils, this extraction procedure can overestimate Ca^{2+} due to dissolution processes, whereas Mg^{2+}, Na^{+}, and K^{+} are not significantly affected (Lalitha et al., 2026). Therefore, because the Ca^{2+} concentrations led to a cation balance with base saturation exceeding 100%, the cation balance was adjusted by setting base saturation to 100%, which required recalculating the Ca^{2+} value. The concentrations of Mg^{2+}, Na^{+} and K^{+} were not modified. Total carbon (C_{tot}), and C_{org} of the soils before and after the experiment were determined on homogenised soil samples following the method of Nieuwenhuize et al. (1994), and soil IC was determined by subtracting C_{org} from C_{tot} (analytical error <0.05%).

2.3 Key parameter calculations

To avoid an overestimation of organic alkalinity (Rieder et al., 2026), the IC-Sink was based on carbonate alkalinity (CA) that was derived from measured values of DIC, pH, temperature, and cation concentrations using PhreeqC (Parkhurst and Appelo, 2013) (database: phreeqc.dat). The total carbon sink (C-$Sink_{pot}$) is the sum of the potential, stoichiometric sinks from

pyrogenic carbon (PyC-Sink$_{pot}$), which reflects C_{org} sequestration from biochar C_{org}, , and inorganic carbon (IC-Sink$_{pot}$) which reflects IC sequestration derived from CA, as the maximum possible alkalinity provided by minerals and biomass upon complete release. The same definitions apply to the actual measured C-, PyC- and IC-Sinks. The calculations of all C-Sinks, the total chemical fluxes and net CA production rates (CA_{prod}) of soil amendments were adapted from Vorrath et al. (2025) (equations 1-8, supplementary information S6). Values of the CA_{prod} after week 39 were used to extrapolate the duration of positive net fluxes (compared to the control) and the corresponding degree of mineral weathering achieved at this time (supplementary information S6). In general, values measured from the control were subtracted from all other values to display the net fluxes. All C-sinks refer to one ton of soil amendment.

To identify synergistic effects, we first determined the *expected* values of the total C-Sink and IC-Sink by adjusting measured values of individual amendments according to the amount of rock or biochar in each soil column. We then calculated the deviation of measured total C-Sink and IC-Sink from the expected values (equations 9-11, details in supplementary information S6). To determine the deviation between expected and measured geogenic IC-Sink, the cation release and resulting IC-Sink from biochar was treated as a constant and the remaining IC-Sink was attributed to mineral weathering (equation 12, supplementary information S6). Further, the budgets of carbon and major cations in the soil were calculated to evaluate changes in these budgets during the experiment (equations 13-16, supplementary information S6). For trace metal fluxes, the deviation of measured from the expected fluxes were determined in the same way as for the C-Sinks (equation 17, supplementary information S6).

3 Results

3.1 RE-biochar characterization

The basic properties of RE-biochars produced by dry-mixing and wet-impregnation, compared to the pure biochar are shown in Table 2 (more details in supplementary data D5). The pure biochar has a C_{org} content of 75.7% and an H:C_{org} molar ratio of 0.30. Compared with pure biochar, all RE-biochars showed lower C_{org} contents (61.2-67.4%), higher H:C_{org} ratios (between 0.45-0.56) and because of the weight loss of biomass during pyrolysis the rock content of RE-biochars increased to 61.2-67.4%. Pure biochar has a BC_{HyPy} content of 71.9 wt% C_{org} and a C_{org} conversion of 37.2%. For RE-biochars, the highest C_{org} conversion (41.6 wt% C_{org})

was reached by the wet-impregnated basanite-enhanced RE-biochar and the highest BC_{HyPy} (85.5 wt% C_{org}) was observed in the wet-impregnated concrete-enhanced RE-biochar.

In the wet-impregnation procedure, using steel slag led to the highest values of dissolved Ca^{2+} and Mg^{2+} in dry biomass (data in supplementary data D6) and the highest increase of C_{org} conversion (7.0%) compared to the dry-mixing process. Our results show that increases in C_{org} conversion in RE-biochars prepared with wet-impregnation of biomass are correlated to Mg^{2+} concentrations in the dry biomass after wet-impregnation, following a strong exponential relationship (r^2=0.9984, Figure 2).

Table 2: The basic characterization of pure biochar and RE-biochars from dry-mixing and wet-impregnation including the C_{org}, rock and biochar content, H:C_{org} molar ratio, the fraction of stable polycyclic aromatic carbon (BC_{HyPy}), biomass C_{org} conversion and the load of dissolved Ca^{2+}, Mg^{2+}, K^+ and Na^+ per kilogram dry biomass added via mineral suspension within the wet-impregnation procedure. BC_{HyPy} and biomass C_{org} conversion values above the reference biochar are indicated in bold. Measurements based on n=1 representative sample.

	C_{org}	Rock	Biochar	H:C_{org} molar ratio	BC_{HyPy}	C_{org} conversion
	%	wt%	wt%		wt%	wt%
Biochar	75.7		100.0	0.30	71.9	37.2
ConcreteChar-dry	28.2	62.9	37.1	0.55	**81.8**	36.4
ConcreteChar-wet	25.8	65.5	34.5	0.56	**85.5**	36.4
SteelslagChar-dry	28.1	65.6	34.4	0.47	**73.2**	32.8
SteelslagChar-wet	29.3	65.3	34.7	0.49	71.6	**39.8**
BasaniteChar-dry	28.5	64.6	35.4	0.51	**72.6**	**40.4**
BasaniteChar-wet	26.1	67.4	32.6	0.51	**79.0**	**41.6**
PeridotiteChar-dry	29.5	62.1	37.9	0.53	60.9	34.0
PeridotiteChar-wet	29.1	63.2	36.8	0.45	**72.0**	**39.2**

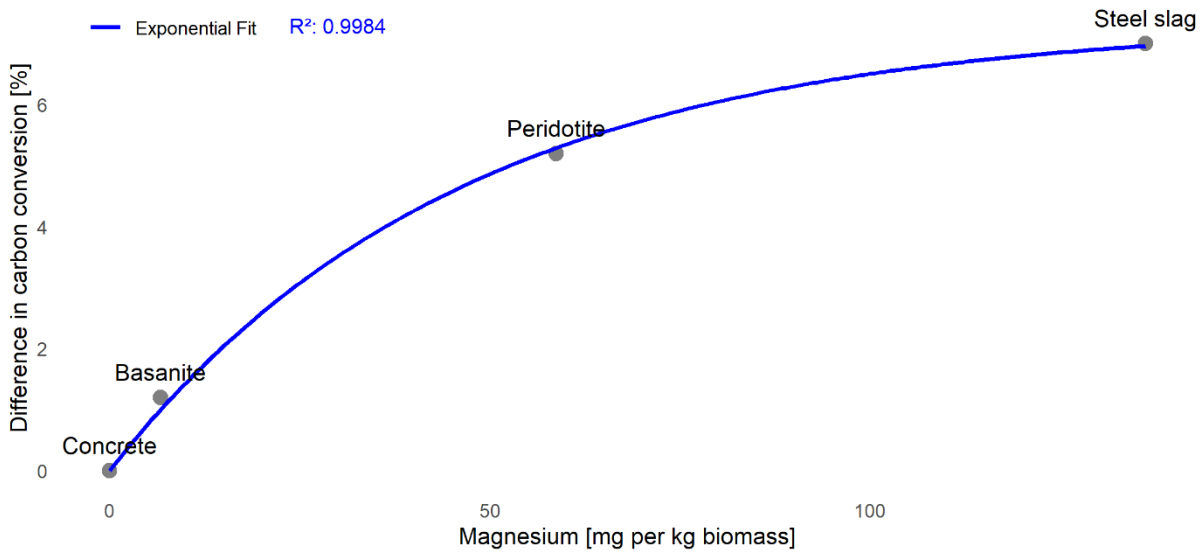

Figure 2: The exponential fit of magnesium concentration in the dry biomass and the difference in C_{org} conversion between dry-mixed and wet-impregnated RE-biochars.

3.2 Leachate chemistry

3.2.1 Carbon and cation fluxes

The results of the total net fluxes are displayed in Figure 3, and show the CO_2 fluxes per ton of amendment for the IC-Sink and DOC, major cations and DSi (data in supplementary data D7). Across all treatments, the IC-Sink is primarily controlled by amendment mineralogy: silicate-rich materials (basanite, peridotite) show the lowest IC-Sinks, whereas limestone and industrial materials (concrete, steel slag) exhibit the highest values (IC-Sink values see Table 6). In co-applications, IC-Sinks are balanced between the mineral feedstocks and the biochar, whereas they are generally lower in RE-biochars, except for the peridotite-based RE-biochars, which show comparatively high IC-Sinks. Concrete and limestone amended columns show a net retention of DOC (14.7 kg CO_2 t^{-1} for concrete and 12.2 kg CO_2 t^{-1} for limestone), while silicates, steel slag and biochar release DOC (up to 33.9 kg CO_2 t^{-1} for steel slag). Fluxes of Ca^{2+} are highest for pure application of limestone and industrial materials (up to 20.8 kg t^{-1}), while biochar and amendments with silicates show a net retention of Ca^{2+} down to -1.3 kg t^{-1}. Mg^{2+} fluxes are highest for all peridotite amendments, while RE-biochars with peridotite stand out with up to 11.7 kg t^{-1} Mg^{2+}. Net negative Mg^{2+} fluxes are present for applications of pure steel slag and its co-application with biochar. K^+ fluxes are clearly dominated by biochar (20.2 kg t^{-1}) in all treatments, while the pure steel slag application shows a K^+ retention of 1.3 kg t^{-1}. Na^+ fluxes are highest for amendments including basanite, with up to 4.5 kg t^{-1}. A retention of DSi

is observed in treatments of steel slag, pure biochar and limestone, while pure basanite, peridotite and concrete show the highest release with up to 7.2 kg t^{-1}. Similar DSi fluxes also appear in RE-biochars with peridotite (up to 6.2. kg t^{-1}).

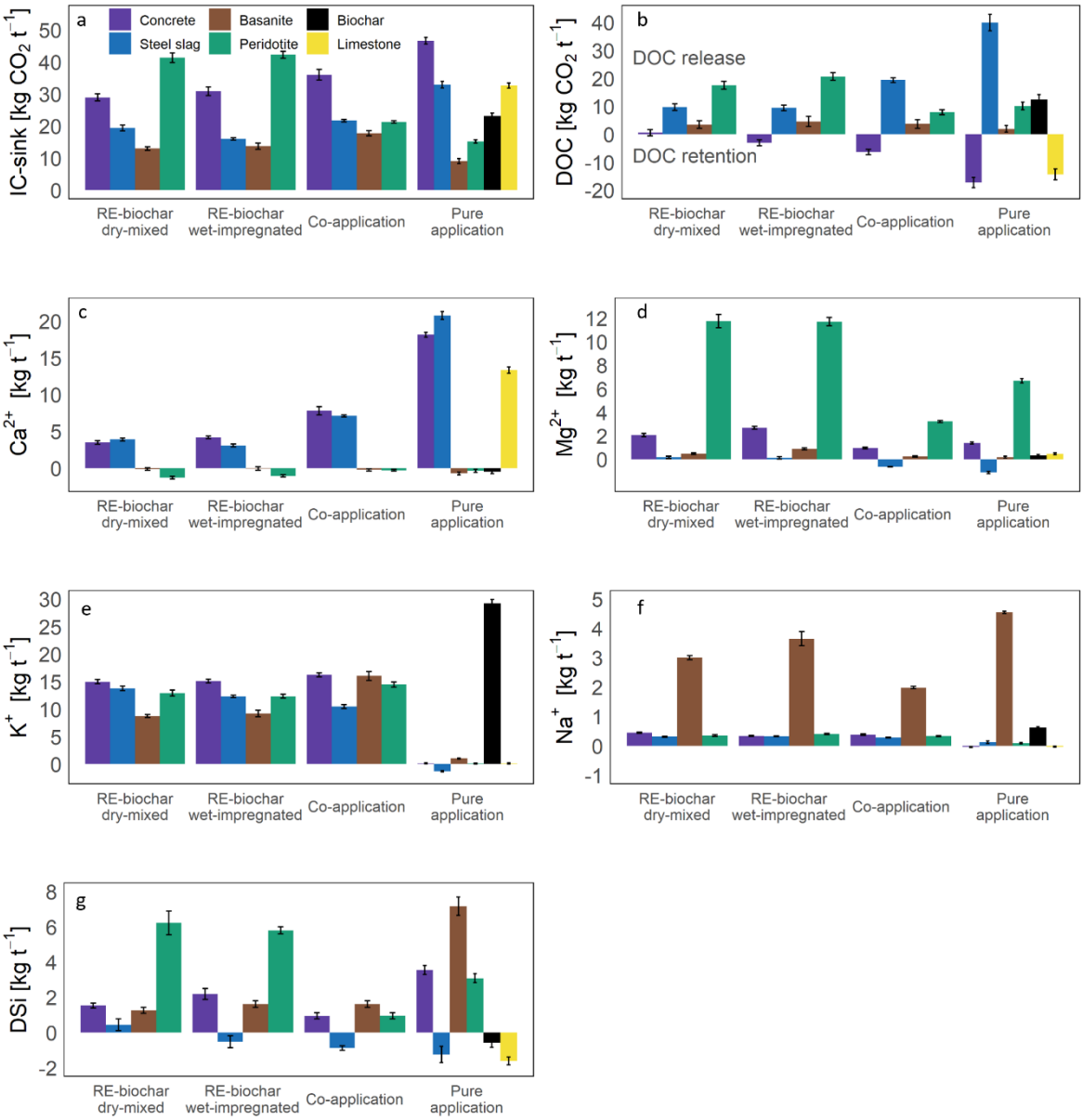

Figure 3: Total net fluxes over 75 weeks calculated from the experiment of a) the IC-Sink, b) dissolved organic carbon (DOC), c) calcium (Ca^{2+}), d) magnesium (Mg^{2+}), e) potassium (K^{+}), f) sodium (Na^{+}), and g) dissolved silica (DSi). The units refer to one ton of material (or material combination). Error bars indicate standard deviation (n=2).

The extrapolation of weekly net CA_{prod} shows continued positive CA_{prod} fluxes between 160 and 2022 weeks (i.e. 3 to 39 years) after the end of the experiment (Table 3). This leads to a

complete dissolution of concrete, while only 2.6-9.1% of the IC-Sink$_{pot}$ of the other amendments would be realized.

Table 3: The extrapolation of net positive alkalinity fluxes based on experimental data from pure mineral amendments with the experimental IC-Sink, the maximum positive alkalinity production based on a linear extrapolation and the resulting extrapolated IC-Sink. The sum of both IC-Sinks is taken to display the released IC-Sink based on the individual IC-Sink potential. The extrapolation for concrete had to be cut off in week 2022 as the IC-Sink$_{pot}$ reached 100%.

Mineral	Experimental IC-Sink	Maximum positive alkalinity production	Extrapolated IC-Sink	Summed IC-Sink	IC-Sink potential	Released IC-Sink
	kg CO_2	weeks	kg CO_2	kg CO_2	kg CO_2	%
Concrete	46.6	2022	670.0	716.6	716.7	100.0%
Steel slag	32.9	160	12.0	44.9	774.8	5.8%
Basanite	9.0	524	22.2	31.2	450.6	6.9%
Peridotite	15.2	234	6.8	22.0	998.8	2.2%
Limestone	32.6	390	44.7	77.2	851.8	9.1%

3.2.2 Trace metal fluxes and retention

Trace metal concentrations declined markedly between week 9 and week 27 and show a strong mineral-specific behaviour where some RE-biochars, certain co-applications and even the control soil have elevated releases exceeding German Drinking Water Ordinance limits (details in supplementary information S7 and supplementary data D8).

Trace metal retention was determined for the first sampling interval and varied substantially among the different soil amendments (

Table 4, supplementary information S6, eq. 17). Overall, 60% of the co-applications show a clear retention, whereas RE-biochars displayed limited retention or even increased releases. The most consistent retention across metals is observed for concrete RE-biochars for Cr, Cu and Ni. Peridotite amendments show mixed effects, while basanite and steel slag amendments have retained several trace metals except for Ni. In general, Cu retention is evident in all co-applications. These deviations from expected values underline that trace

metal retention is highly mineral-specific, with synergistic effects in co-applications evident in some cases but absent or even counterproductive in others.

Table 4: The deviation of trace metal fluxes from measured to expected net values (%) in mineral-biochar co-applications and co-pyrolysis of biomass with minerals based on dry-mixing and wet-impregnation. Green fields indicate a retention of trace metals.

Configuration	Cd	Cr	Cu	Ni	Pb
ConcreteChar-dry	26.64	< -100	-53.16	> 100	13.88
ConcreteChar-wet	39.66	< -100	-31.26	< -100	2.13
Concrete + Biochar	< -100	13.94	< -100	< -100	> 100
SteelslagChar-dry	85.34	> 100	68.70	> 100	79.36
SteelslagChar-wet	87.86	> 100	72.87	91.63	83.39
Steel slag + Biochar	> 100	-13.36	< -100	36.63	< -100
BasaniteChar-dry	35.57	> 100	14.21	> 100	7.94
BasaniteChar-wet	48.18	-6.76	23.02	> 100	25.27
Basanite + Biochar	-22.20	> 100	-41.02	> 100	-49.67
PeridotiteChar-dry	40.17	> 100	21.83	< -100	32.18
PeridotiteChar-wet	47.69	< -100	22.83	< -100	35.96
Peridotite + Biochar	-57.11	93.26	-97.66	6.14	-71.33

3.2.3 Soil cation budgets

The net cation budget, after correction for the control soil, represents the distribution pathways of cations that were released from the input materials either to the exchangeable fraction or the leachate water (Table 5, figure in the supplementary information S8 and more details in the supplementary data D9). In general, 2.2-14.7% of cations from the input materials are present in the leachate water and 0.2-2.1% in the exchangeable fraction, while the pure biochar amendment is a clear exception that released 57.8% of its major cations to the leachate and 2.0% to the exchangeable fraction. A redistribution of soil inherent cations during the experiment (from soil mineral dissolution and immobilization) may be masked by cations from input materials. Further, some values are above 100% or below -100%, which is a clear indicator of the involvement of cations other than from the input material. Taking into account the maximum possible stoichiometric cation release, between 84.1 and 98.6% of major cations remain in the input material (or other solid soil pools), with an exceptional cation release of 65.7% from pure biochar. Negative values indicate a loss of the specific cation from either the exchangeable fraction or leachate.

Table 5: The net cation budget of the soil determined related to the input material (%) from cations in the soil exchangeable fraction and leachate. Cells with “+” and “-“ are cases where specific cations

were not added by the input material but positive or negative net values appeared in the samples, respectively. Green fields present values above 100%, indicating mobilized cations from the soil, grey fields are negative values that indicate the retention of cations in the soil. To avoid an overestimation of cation release from the input materials, values of K^+ and Na^+ above 100% were set to 100% of the input material to calculate the corrected remaining material.

Configuration	ConcreteChar-dry	ConcreteChar-wet	Concrete + Biochar	Concrete	SteelslagChar-dry	SteelslagChar-wet	Steel slag + Biochar	Steel slag	BasaniteChar-dry	BasaniteChar-wet	Basanite + Biochar	Basanite	PeridotiteChar-dry	PeridotiteChar-wet	Peridotite + Biochar	Peridotite	Biochar	Limestone
Exchangeable cations %																		
Ca2+	0.2	-0.1	1.1	1.2	0.0	0.3	0.5	0.4	-0.1	0.6	0.3	0.3	-25.0	-26.8	-11.6	-187.0	-6.2	0.9
Mg2+	2.7	0.4	2.8	0.7	2.1	1.6	4.2	1.3	0.6	1.2	2.0	0.5	0.2	0.2	0.4	0.1	18.1	-2.3
K+	4.2	18.9	-4.2	-32.9	24.5	9.3	19.2	+	-0.5	0.0	0.4	1.9	50.3	57.2	21.9	2553.0	13.3	-88.4
Na+	113.6	0.2	120.2	1050.2	487.4	117.4	0.2	+	7.0	0.0	3.4	0.0	-1099	-1411	-99.0	-	-148.4	+
Sum	1.0	0.5	1.5	2.1	1.6	0.9	1.8	1.5	0.7	0.8	1.2	0.4	0.2	0.3	0.3	0.3	2.0	1.2
Leached cations %																		
Ca2+	1.5	1.7	4.2	5.4	1.3	1.0	3.7	5.9	-0.6	-0.3	-0.7	-0.9	-14.4	-12.7	-3.3	-22.1	-3.1	3.1
Mg2+	15.1	19.3	8.1	8.2	0.1	-0.1	-3.9	-4.4	1.1	2.1	0.6	0.3	6.6	6.3	2.1	2.3	3.7	13.2
K+	193.6	207.8	166.1	14.4	208.4	184.2	110.9	-	54.0	57.6	96.5	6.3	175.5	171.3	155.1	59.5	158.8	19.4
Na+	106.6	84.6	75.9	-17.1	140.0	141.8	66.7	+	41.4	48.5	31.3	38.2	520.3	773.5	80.9	+	75.0	-
Sum	10.0	10.2	13.3	5.7	6.8	6.0	7.7	4.4	9.4	10.6	14.7	3.6	10.4	10.0	7.7	2.2	57.8	3.3
Released cations %	11.0	10.8	14.8	7.7	8.4	6.9	9.5	5.8	10.1	11.4	15.9	4.1	10.6	10.3	8.1	2.6	59.8	4.5
Corrected remaining material %	92.9	93.3	88.8	93.2	95.9	95.8	91.8	94.2	89.9	88.6	84.1	95.9	92.6	92.8	94.8	98.6	65.7	96.0

3.3 C-Sinks from different soil amendments

The total C-Sink$_{pot}$ ranges between 451 and 2801 kg CO_2 t^{-1} for basanite and biochar, respectively (Table 6). Biochar provides the highest C-Sink$_{pot}$ (2801 kg CO_2 t^{-1}) due to its high C-Sink:mass ratio, while the mass-based C-Sink$_{pot}$ of mineral feedstocks is generally lower at 383 to 999 kg CO_2 t^{-1} material. Co-applications achieve a C-Sink$_{pot}$ of 1632 to 1904 kg CO_2 t^{-1} whilst RE-biochars range from 1261 to 1697 kg CO_2 t^{-1} material.

The experimentally determined actual C-Sinks based on the calculated PyC-Sink and IC-Sink from leachate water analyses range from 9.0 kg CO_2t^{-1} (basanite) to 46.6 kg CO_2 t^{-1} (concrete) for pure mineral amendments but increases to around 1038 kg CO_2 t^{-1} for co-applications and to 874.4 kg CO_2 t^{-1} for RE-biochars (Table 6). The deviation of the measured from the expected total C-Sink is between -1.7 and 3.4% for RE-biochars and co-applications. In RE-biochars, the measured IC-Sinks are generally lower than the expected IC-Sinks, except for wet-impregnated

basanite RE-biochar showing a slight increase, and peridotite RE-biochars standing out with an up to 133.6% higher IC-Sink. Except for steel slag (-22.6%), co-applications also show a higher measured IC-Sink. The deviation for the geogenic IC-Sink or the value of accelerated/suppressed weathering is similar, with negative values of -63 to -17.6% for RE-biochars and the co-application with steel slag, while the other RE-biochars and co-applications are positive, with peridotite RE-biochars showing remarkable accelerated values of up to 251.7%.

Table 6: The C-Sink potentials and actual C-Sinks from the experiment of all RE-biochars, co-applications and pure amendments are reported as the C-Sink, the inorganic carbon sink (IC-Sink) and the pyrogenic carbon sink (PyC-Sink). The deviation of the measured from the expected C-Sinks and IC-Sinks is expressed as percentage. The deviation of the measured from expected geogenic IC-Sink refers to the IC-Sink solely occurring from mineral weathering (calculated after equations 9-12, supplementary information S6).

		C-Sink potential			**C-Sink from experiment**			**Deviation**		
	Column Material	C-Sinkpot	IC-Sinkpot	PyC-Sinkpot	C-Sink	IC-Sink	PyC-Sink	C-Sink	IC-Sink	Geogenic IC-Sink
		kg CO2 t-1			kg CO2 t-1			%		
RE-biochar	ConcreteChar-dry	1657.2	623.2	1034.0	874.4	28.9	845.4	**-1.0**	**-23.7**	**-30.5**
	ConcreteChar-wet	1597.0	651.0	946.0	839.4	30.9	808.5	**-0.9**	**-19.9**	**-25.0**
	SteelslagChar-dry	1575.1	544.8	1030.3	773.6	19.4	754.2	**-1.3**	**-34.2**	**-46.8**
	SteelslagChar-wet	1627.5	553.2	1074.3	785.5	16.0	769.6	**-1.7**	**-45.9**	**-63.0**
	BasaniteChar-dry	1328.5	283.5	1045.0	771.5	13.0	758.5	**-0.1**	**-28.4**	**-17.6**
	BasaniteChar-wet	1261.4	304.4	957.0	769.8	13.7	756.1	0.0	0.7	1.6
	PeridotiteChar-dry	1697.0	615.3	1081.7	700.1	41.4	658.7	3.4	127.6	245.7
	PeridotiteChar-wet	1691.0	624.0	1067.0	810.0	42.3	767.7	3.1	133.6	251.7
Co-application	Concrete + Biochar	1763.9	369.1	1394.8	1038.3	36.0	1002.3	0.1	3.3	5.0
	Steel slag + Biochar	1792.8	398.0	1394.8	1024.0	21.7	1002.3	**-0.6**	**-22.6**	**-38.4**
	Basanite + Biochar	1631.5	236.7	1394.8	1020.0	17.7	1002.3	0.2	10.4	37.1
	Peridotite + Biochar	1904.2	509.4	1394.8	1023.5	21.2	1002.3	0.2	11.1	27.9
Pure amendments	Concrete	716.7	716.7	0.0	46.6	46.6	-			
	Steel slag	774.8	774.8	0.0	32.9	32.9	-			
	Basanite	450.6	450.6	0.0	9.0	9.0	-			
	Peridotite	998.8	998.8	0.0	15.2	15.2	-			
	Biochar	2800.6	24.9	2775.7	1994.5	23.1	1994.5			
	Limestone	851.8	851.8	0.0	32.6	32.6	-			

4 Discussion

4.1 Impact of co-pyrolysis on C_{org} conversion and biochar stability

Our results demonstrate an exponential relationship between C_{org} conversion and dissolved Mg^{2+} concentrations in biomass feedstocks (r^2=0.9984, Figure 2) where wet-impregnation

with steel slag produces the highest increase of C_{org} conversion (7.0%) after adding 0.014 wt% of dissolved Mg^{2+} to the dry biomass prior to pyrolysis (Figure 2). This aligns with several studies showing that dry-mixing with magnesium before pyrolysis markedly enhances carbon retention in biochar. For example, Zhu et al. (2023) report that 1 wt% Mg^{2+} (as $MgCl_2$) increases C_{org} conversion by more than 12%, which is likely attributed to the catalytic role of Mg^{2+} in suppressing volatile formation during thermal decomposition (Yu et al., 2014). Higher C_{org} conversion has also been linked to the formation of MgO and magnesium carbonate phases that sorb small (volatile) low molecular weight carbon compounds and form protective barriers against oxidation (Nan et al., 2020). Compared to other cations, Mg^{2+} consistently appears as the most effective additive for improving C_{org} conversion (Nan et al., 2020). Although Ca^{2+} has also been associated with increased carbon content (Li et al., 2014), no significant effect was detected in this study.

Despite the strong influence of Mg^{2+} in wet-impregnated treatments, the pure biochar still shows a higher C_{org} conversion (37.2%) than RE-biochars with concrete or dry-mixed RE-biochars with steel slag and peridotite (Table 2). Peridotite contains the highest amount of MgO (45.6 wt%) present mainly in the minerals olivine and serpentine, yet the corresponding dry-mixed RE-biochar has a low C_{org} conversion efficiency. Likely, the form of Mg^{2+}, either bound within a crystal lattice of a mineral or dissolved in water, plays a crucial role affecting Mg^{2+} catalytic activity. Basanite derived RE-biochars show a generally higher C_{org} conversion, independent from the mixing procedure, which is contrary to other studies (Meyer zu Drewer et al., 2025).

Previous studies suggested increases in C_{org} stability when biomass was co-pyrolysed with mineral additives, but consistent experimental evidence has been lacking (Buss et al., 2022; Meyer zu Drewer et al., 2025, accepted). In our study, hydropyrolysis revealed a higher percentage of BC_{HyPy} for most RE-biochars except those mixed with peridotite (Table 2Table 2**Fehler! Verweisquelle konnte nicht gefunden werden.**). Although the high Ca content in concrete (41.7 wt% CaO) can be clearly associated with higher BC_{HyPy}, this relationship is not present for steel slag, despite its similarly high Ca content (45.1 wt% CaO). We propose that this contrast may stem from different minerals containing the bulk of the calcium, which is calcite for the concrete and Ca-silicates, and oxides and hydroxides for the steel slag (supplementary data D2). Although concrete mainly contains calcium carbonates that may decompose during pyrolysis, our thermogravimetric analysis did not show decarbonation that

would have made CaO available to promote carbon stabilization (supplementary data D3). The only mineral that could have provided CaO during pyrolysis is portlandite, but its content was likely too low (0.2%) to have a substantial effect on biochar stabilization. In steel slag, calcium is predominantly found in the form of calcium silicates and calcium iron oxides, which likely remain inert during pyrolysis and therefore do not influence carbon stability. Conversely, steel slag also contains 10.2% portlandite, yet this comparatively high abundance still does not enhance C_{org} stability, directly contradicting our earlier expectation that portlandite-derived CaO would increase biochar stabilization. Overall, our results regarding concrete RE-biochars fit earlier findings showing that calcium carbonates promote carbon stabilization attributed to matrix aromatization during pyrolysis (Li et al., 2014), while the effects of calcium silicates, calcium iron oxides, and calcium hydroxides remain unresolved.

4.2 C-Sinks from different soil amendments in a sandy soil

4.2.1 IC-Sinks from mineral weathering

The IC-sinks developing from pure mineral amendments and based on leachate analyses, show a realization of 1.5% (peridotite) to 6.5% (concrete) of the stoichiometric IC-$Sink_{pot}$ over 17 months with the order of fastest weathering being: concrete > steel slag > limestone > basanite > peridotite (Table 6). Fast weathering can mainly be attributed to the presence of the minerals calcite (concrete, steel slag, limestone), portlandite and larnite (steel slag), nepheline and leucite (basanite) and olivine (peridotite, basanite). A similar order has been found by Hammes et al. (2025) in a large-scale greenhouse pot experiment, where only the order of basanite and peridotite were reversed. The release of 4.2% IC-$Sink_{pot}$ from steel slag is comparable to previous findings under similar conditions, where 1.6% of the IC-$Sink_{pot}$ was released over 15 months in a plant-inclusive pot experiment (Steinwidder et al., 2026). Peridotite shows a lower release compared with a 2-month pot experiment, where values were 3.4 times higher (Te Pas et al., 2026). An ERW field study using returned concrete in Ireland yielded up to 2.7% of the IC-$sink_{pot}$ over 11 months, including plants and non-carbonic acid weathering contributions (McDermott et al., 2024). Many pot and mesocosm studies report low to negligible alkalinity release from basaltic amendments due to unfavourable water conditions, plant presence, or soil-cation interactions (Buckingham and Henderson, 2024; Steinwidder et al., 2026; Vienne et al., 2022, 2024, 2026b). Together, these comparisons emphasise that observed weathering rates depend not only on mineral composition but also

on the temporal window captured by the experiment, with early pulse effects often overestimating long-term release.

In contrast to short experiments of less than one year (e.g. Vorrath et al., 2025), our 17-month experiment enabled us to separate the initial alkalinity release of fast weathering dust particles and mobile cations and to observe stabilised CA_{prod} fluxes after week 39. This allowed us to extrapolate the continuation of long-term, reduced weathering fluxes (Table 3). Although we acknowledge that a linear model does not fully capture the complexity of mineral weathering in the soil, it provided the best fit for our measured fluxes (supplementary information S6, Table S2), and therefore the resulting extrapolation should not be viewed as definitive. While concrete would have been completely weathered after 40 years, steel slag, basanite, peridotite, and limestone would have released 2.2-9.1% of their IC-$sink_{pot}$ until CA_{prod} fluxes were equal to the control. This suggests that, under most conditions, the release of the full IC-$sink_{pot}$ is unlikely to be captured by leachate alkalinity monitoring. Alkalinity losses can generally occur due to secondary mineral formation (Dietzen and Rosing, 2023; Niron et al., 2024; Steinwidder et al., 2026; Te Pas et al., 2026, 2025), plant uptake of cations (Kantola et al., 2023; Rijnders et al., 2023; Vienne et al., 2026a), cation sorption to organic surfaces and MAOM formation (Buss et al., 2024; Te Pas et al., 2026; Vienne et al., 2026a), and mineral surface passivation (Oelkers et al., 2018). These alternative cation pathways illustrate uncertainties in their contribution to alkalinity generation over time.

4.2.2 C-Sink from biochar and combined applications

In biochar, the main contributor to the total C-$Sink_{pot}$ originates from the PyC-Sink, whereas its IC-sink is minor and does not contribute additional carbon sequestration, and therefore does not provide CDR (Vorrath et al., 2025). While IC-Sinks from minerals develop slowly, more than 93% of the biochar IC-Sink is released after week 75 (and 98% after week 87) (Table 6) which highlights the importance of our long incubation period, capturing nearly the complete release of biogenic cations and its IC-$Sink_{pot}$. This temporal pattern shows that biochar mainly contributes to high alkalinity fluxes in the early stage of our experiment and is only a minor contributor to low, long-term alkalinity fluxes in the second year. As minerals have relatively small C-$Sink_{pot}$:mass ratios, the C-$Sink_{pot}$ of co-applications and RE-biochars is defined by the contributions of each material, but it is not proportional to the biochar content. For example, the 1:1 co-application of basanite and biochar provides a C-$Sink_{pot}$ of 1631 kg CO_2 t^{-1}, about 300 kg CO_2 t^{-1} higher than the corresponding RE-biochars containing 34 wt%

biochar. On the other side, a 1:1 co-application also exceeded the corresponding RE-biochar C-sink$_{pot}$ by 110-170 kg CO_2 t^{-1} although the biochar content was 69 wt% (Vorrath et al., 2025). This indicates that the pyrogenic carbon contribution in RE-biochars is lower than its proportional share. Although wet-impregnated feedstocks show higher C_{org} conversion rates (Table 2), the variability of C_{org} across materials prevents clear attribution of potential effects of mixing procedures on the C-sink$_{pot}$ or experimental C-sink.

During the 75-week incubation, the different temporal behaviour of biochar and mineral amendments became evident. In contrast to mineral weathering, where the IC-sink increases over time, biochar undergoes aging, meaning that the PyC-Sink of biochar decreases due to decomposition of labile organic carbon fractions from microbial activity and surface oxidation (Azzi et al., 2024; Sanei et al., 2025). Our BC_{HyPy} content of 71.9% of C_{org} (Table 2) is low compared with typical values of woody biochars and RE-biochars at 650 °C (BC_{HyPy} above 90%) (Meyer zu Drewer et al., 2025). Biochar stability is strongly influenced by feedstock composition (Ippolito et al., 2020), with lignin-rich biomasses producing more stable biochars (Ma et al., 2019). Thus, the use of protein-rich soybean meal (Karr-Lilienthal et al., 2004) alongside spruce in our study likely explains the lower stability observed here. Nevertheless, over longer timescales, decreases in the PyC-Sink may be partially offset by increases in the IC-Sink, resulting in a complementary and sustainable CDR portfolio (Meyer zu Drewer et al., accepted; Rueda et al., 2021; Vorrath et al., 2025). Such opposing time trajectories in the IC- and PyC-Sink development underscore why long incubations are essential to understand how the fate of labile C_{org} from biochar can eventually be counterbalanced by the IC-Sink. Overall, co-application appears more practical and economical because of fewer production steps and offers a high C-Sink$_{pot}$ per mass, while co-pyrolysis can increase C_{org} stability.

4.2.3 Synergistic effects on the total C-Sink and the role of geogenic cations

The combined effects of mineral weathering and biochar addition can be interpreted via several processes in which dissolution, cation exchange, sorption to biochar surfaces, and secondary mineral formation jointly determine the observed C-Sinks. The relative importance of these processes depends strongly on the mineral composition and on whether biochar and mineral are combined by co-application or co-pyrolysis. Expected C-Sinks based on pure amendments were compared with experimental outcomes to evaluate synergistic/antagonistic effects (Table 6). For both co-applications and RE-biochars, the deviation of measured from expected total C-Sink remains below 3.4%, indicating limited

552 synergistic or antagonistic effects from combining geochemical and pyrogenic CDR. The
553 deviation of the measured IC-Sink only captures deviations from combined mineral
554 weathering and pyrogenic carbon, while the deviation of the measured geogenic IC-Sink
555 indicates whether mineral weathering itself is accelerated or reduced. Both metrics show
556 consistent patterns: in RE-biochars, combinations with concrete, steel slag, and dry-mixed
557 basanite result in reduced IC-Sinks; wet-impregnated basanite does not alter the IC-Sink; and
558 peridotite RE-biochars show remarkably higher IC-Sinks. In co-applications, the IC-Sinks are
559 enhanced for concrete, basanite, and peridotite, whereas steel slag shows a reduced IC-Sink.
560 These results demonstrate that simple addition of IC-Sinks from single mineral powder and
561 biochar applications does not accurately mirror the actual leaching of major cations measured
562 in RE-biochars.

563 Since more than 90% of biochar's IC-Sink was released within 17 months (Table 6), the
564 geogenic IC-Sink in combined amendments can be conservatively estimated by simply
565 subtracting the biochar IC-Sink$_{pot}$. Previous studies reported no increase in IC-Sinks for
566 co-applications of biochar and basanite (Honvault et al., 2024; Vorrath et al., 2025), while
567 slight increases were observed for peridotite (Te Pas et al., 2026). Such comparisons of
568 synergistic effects across different soils remain difficult as effects are found to be strongly soil-
569 dependent (Hammes et al., 2025; Vorrath et al., in prep.). For RE-biochars, suppressed mineral
570 weathering due to pyrogenic coatings on mineral surfaces has been hypothesised (Meyer zu
571 Drewer et al., 2025) but not experimentally confirmed (Meyer zu Drewer et al., accepted).
572 CaO production via thermal alteration of minerals in steel slag and concrete is also unlikely, as
573 our thermogravimetric analyses showed weight loss that can be mainly attributed to a loss of
574 water (supplementary data D3). In contrast, the substantially higher measured geogenic
575 IC-Sink of peridotite RE-biochars (up to +251.7%) can be explained by thermal activation of
576 serpentine minerals during pyrolysis (see chapter 4.3.3). In most co-applications (except for
577 steel slag), our observations indicate that sorption surfaces introduced by biochar addition do
578 not delay or reduce the IC-Sink by cation scavenging from soil solution (Planavsky et al., 2024).
579 Instead, they support the concept that biochar improves weathering conditions (Amann and
580 Hartmann, 2019; Meyer zu Drewer et al., 2025; Vorrath et al., 2025). The strong decrease of
581 steel slag weathering in the co-application may be linked to interactions between dissolved
582 calcium silicates and pyrogenic carbon (see chapter 4.4). We suggest, that in general, biochar
583 may act as either an accelerator or inhibitor of mineral weathering, depending on the mode

584 of combination. In co-applications, biochar may modify soil solution chemistry through cation
585 retention and sorption and thereby sustain mineral weathering. In RE-biochars, minerals may
586 be embedded in the biochar matrix, so pyrolysis can either suppress weathering by reducing
587 mineral surface exposure or, for serpentine-rich materials, increase reactivity through thermal
588 activation. Thus, the material-specific responses can still overprint general response patterns
589 from co-application and co-pyrolysis as the direction of the effect depends on mineral
590 composition and pyrolysis-induced transformations.

591 Considering these synergistic patterns, a qualitative assessment of the different materials
592 suggests that single applications and co-applications of biochar with all mineral feedstocks
593 offer the most promising performance in the studied sandy soil (supplementary information
594 S9). These combinations align with the experimentally observed non-additive behaviour of the
595 enhancement of measured geogenic IC-Sinks for concrete, basanite and peridotite
596 co-applications, and benefit from biochar's capacity to retain DOC and improve weathering
597 conditions (Figure 3). Overall, the substantial reduction of DOC leaching with pure concrete
598 and in co-application with biochar could counterbalance possible CO_2 efflux effects from non-
599 carbonic acid weathering (West and McBride, 2005). In contrast, RE-biochars combined with
600 steel slag or basanite appear less favourable, as they tend to suppress mineral weathering and
601 do not mitigate DOC losses, despite the strong thermally activated weathering observed for
602 peridotite RE-biochars. Although trace metal release was not included in this qualitative
603 evaluation, it remains a relevant consideration for field deployment and must be assessed in
604 relation to local soil conditions and regulatory thresholds. Overall, these observations
605 highlight that the suitability of individual minerals depends not only on their IC-$Sink_{pot}$ but also
606 on their interactions with biochar and their broader effects on soil carbon dynamics and
607 practical implementation.

608 Combining ERW and biochar in field applications introduces challenges for monitoring,
609 reporting, and verification (MRV) because the two approaches rely on fundamentally different
610 accounting procedures. Biochar MRV is based on pre-deployment chemical and physical
611 characterisation (e.g. Schmidt et al., 2024), while ERW monitoring requires long-term analyses
612 of soil or leachate samples to quantify mineral dissolution and carbon sequestration (e.g.
613 Isometric, 2025; Rainbow, 2025). Our results show that both, mineral weathering and biochar
614 leaching, release cations and increase soil alkalinity, thereby contributing to an IC-Sink and
615 interfering with standard ERW MRV protocols where soil alkalinity is considered to remain

from geogenic sources only. As our long-term experiment showed the release of nearly the complete biogenic IC-Sink$_{pot}$, subtracting this number from the total alkalinity flux integrated over time provides a simple and feasible estimation of the geogenic alkalinity release and allows the correct accounting of geogenic-derived CDR.

4.3 Chemical fluxes in the soil

4.3.1 Pure amendments

The long duration of our experiment allows a separation of the initial flush of mobile cations and fast weathering of dust particles within the first months and to identify long-term cation release patterns. This is particularly important because the first months capture transient pulse processes not just from weathering but also from soil responses to drying and mixing with oxygen, whereas later phases reflect more stable soil interactions with biochar and ERW and the progressive redistribution of cations among soil pools. Carbonate minerals generally show higher weathering rates than silicates (Lasaga and Berner, 1998), which is reflected in our data where Ca^{2+} from limestone and industrial materials exhibit the highest fluxes (up to 20.8 kg t^{-1}, Figure 3, supplementary data D7). For peridotite, the IC-Sink is mainly driven by Mg^{2+} release from the weathering of olivine, which comprises 63.3% of its composition (supplementary data D2). In basanite, Na^{+} dominates the IC-Sink, likely originating from rapidly weathering Na-rich minerals such as leucite, nepheline, and interstitial glass (Dupla et al., 2025). High DSi fluxes in peridotite and basanite reflect weathering of silicate minerals such as olivine and nepheline, while elevated DSi in concrete likely derives from weathering of calcium silicate hydrates, the dominant binding phase in cementitious materials (Multer Hopkins et al., 2024). Biochar shows a small IC-Sink (23 kg CO_2 t^{-1}), driven primarily by fast leaching of major cations within the first few months, which was also observed in other studies (Ding et al., 2010; Meyer zu Drewer et al., 2025). By far the largest contribution to the IC-Sink of biochar comes from K^{+}, a common pattern observed especially for biochar based on straw biomass, which shows immediate release of K^{+} (Ippolito et al., 2020; Meyer zu Drewer et al., 2025). As fluxes from the control soil are subtracted from all amendments, negative fluxes in the leachate indicate a net retention of certain elements. Retention of Ca^{2+} in silicate amendments coincides with strong Mg^{2+}, Na^{+}, and DSi release (Figure 3, supplementary data D7), suggesting that a high abundance of Mg^{2+} could support the formation of Ca-Mg clay minerals (e.g., kaolinite, montmorillonite) and possibly calcite acting as a Ca^{2+} sink. The

suggested calcite formation coincides with a higher IC content measured in post-experiment soil analysis for peridotite amendments, which is however not evident in basanite-amended soil (supplementary data D10). Other soil columns show a net retention of Mg^{2+}, K^{+} and DSi with steel slag, and DSi retention in limestone amendments which probably indicates illite and vermiculite formation (Hong et al., 2014; Wilson, 1999). The retention of DSi in the pure biochar amendments may be explained by the adsorption of silicic acid by low-silicon biochar (Wang et al., 2018). As secondary mineral formation and cation redistribution may directly impact cation fluxes, this underlines the relevance of long-term experiments (e.g. Hammes et al., 2025).

Overall, the time series of fluxes reflect a temporal transition from rapid release of labile components to slower redistribution and retention processes that can only be resolved over extended incubation periods. The impact of ERW on SOC dynamics has recently gained attention due to the likely increased soil respiration evoked by an upward shift of soil pH, higher plant productivity and microbial activity (Anthony et al., 2025; Buss et al., 2024; Fang et al., 2023). While we did not measure soil CO_2 efflux, we assessed DOC fluxes, which are linked to rapid soil pH shifts (Gao et al., 2025) and may provide an indicator of soil carbon losses, as DOC represents a mobile and reactive pool sourced from soil organic matter decomposition (Camino-Serrano et al., 2016; Kalbitz et al., 2000). Only amendments with concrete and limestone, which mostly contain carbonate minerals, show net DOC retention likely related to the stabilization mechanisms of Ca^{2+} on SOC (Rowley et al., 2018; Setia et al., 2014), while silicates, steel slag, and biochar result in DOC release (Figure 3). Assuming a carbon use efficiency of 70%, meaning that 70% of the DOC found in the leachate water will be respired and converted to inorganic CO_2 in the long run (Sinsabaugh et al., 2013), DOC loss from steel slag would reduce its IC-sink by 85%, down to 4.3 kg CO_2 t^{-1}. Although increases in soil respiration from ERW have been attributed to pH shifts and enhanced microbial activity (Dupla et al., 2024; Su et al., 2025), the highest delta pH values in our experiment, observed for peridotite, steel slag, and concrete, lead to divergent DOC responses (supplementary information S10 and S11). This suggests that DOC leaching due to increased soil respiration might be more complex than suggested and the composition of the dissolving minerals responsible for the pH increase may play an important role as well as later-stage soil-specific responses such as the stabilisation of SOC through calcium cations (Rowley et al., 2018).

Accordingly, the long-term incubation reveals that early DOC pulses and later DOC retention or release are governed by different process combinations, rather than by pH change alone.

While biochar commonly increases CO_2 efflux through decomposition of its labile fraction (Ansari et al., in review; Kammann et al., 2012; Te Pas et al., 2026; Wang et al., 2016, 2014), Chiaravalotti et al. (2025) did not find direct evidence of ERW-induced CO_2 efflux, and DOC dynamics appear more closely tied to soil-specific SOC processes and the Birch effect, the rapid pulse of microbial activity and carbon release that occurs when dry soil is rewetted (Jarvis et al., 2007), rather than to pH alone. Our study confirms the strong impact of the Birch effect as DOC leaching is concentrated in the first year, with more stable flux patterns in basanite, concrete, and limestone treatments during the second year (supplementary information S10, supplementary data D11). Such time-dependent biogeochemical processes become visible only over the long incubation period and indicates that early DOC losses in short-term experiments are dominated by microbial pulse responses, whereas later fluxes reflect more stable amendment–soil interactions. Other studies highlight that ERW can enhance SOC sequestration through MAOM formation exceeding the IC-Sink (Xu et al., 2024), promote IC-to-SOC transformation via (hydr)oxides (Niron et al., 2024), and stabilize existing SOC (Boito et al., 2025; Buss et al., 2024; Steinwidder et al., 2025), while no effect on any soil carbon pools is also evident (Maxbauer et al., 2026).

In our study, DOC responses are not directly linked to high Ca^{2+} fluxes as both retention and leaching occur. For Mg^{2+} from limestone and industrial materials, there seems to be a reverse connection to DOC leaching, where the Mg^{2+} loss from concrete and limestone is associated with DOC retention and the Mg^{2+} retention from steel slag is associated with DOC leaching. This may point towards DOC retention being linked to Mg^{2+} via sorption (Setia et al., 2014) and the Mg^{2+} release from dissolution of 2:1 silicate layer minerals. Slightly elevated SOC contents (up to 0.3% above the control, supplementary data D10) across most amendments likely reflect formation of aluminosilicates, (hydr)oxides, and crystalline minerals, which enhance organo-mineral associations (Liu et al., 2023; Rowley et al., 2018) and may explain a reduced C_{org} loss during the experiment. These patterns do not apply to silicate amendments or biochar. It remains undefined if DOC retention and avoided respiration to inorganic CO_2 presents an additional contribution to the total C-Sink. If attributed to the total C-Sink, DOC retention of concrete and limestone amendments could add up to 44% to the IC-Sink and play a major role in SOC build-up for soils.

Trace metals remain a concern for ERW, particularly for Ni and Cr released from olivine-rich peridotite (Rijnders et al., 2025). Trace metal concentrations in the leachate peak early during the experiment in week 9, likely due to initial high weathering rates overprinting pH-controlled immobilization (Bang and Hesterberg, 2004; Te Pas et al., 2023). When subtracting trace metal fluxes from the control soil, concentrations exceeding German Drinking Water Ordinance thresholds occur for Ni in peridotite and steel slag and for Pb in biochar (supplementary information S7). The latter suggests that that concerns for trace metals must also be considered in biomass-based CDR and background levels of trace metals in the soil may interfere with monitoring following environmental guidelines. Compared with Rijnders et al. (2025) our results from pure basanite are similar for Cd, Ni and Pb, while leached trace metals from concrete and steel slag weathering were much lower due to lower application rates and probably different material compositions. Similar trace metal concentration trends are reported in other studies for steel slag, basanite, and peridotite (Amann et al., 2020; Steinwidder et al., 2026).

4.3.2 Co-application of minerals and biochar

In co-applications, IC-Sinks of silicate minerals and concrete are generally elevated, consistent with synergistic increases in the geogenic IC-Sink (chapter 4.2.3, Table 6). Ca^{2+} fluxes decrease in both concrete and steel slag co-applications, likely indicating the adsorption onto charged biochar surfaces. A delayed DSi flux due to adsorption onto biochar (Wang et al., 2018) may contribute to secondary mineral formation and reduce the IC-Sink, mainly impacting co-applications with concrete and silicate amendments that show large DSi fluxes in general, while this effect hardly occurs for the low DSi release from steel slag (Figure 3). For co-applications with silicates, we observe a lower retention of Ca^{2+} in the soil leading to generally higher IC-Sink and geogenic IC-Sink (Table 6Table 6: The C-Sink potentials and actual C-Sinks from the experiment of all RE-biochars, co-applications and pure amendments are reported as the C-Sink, the inorganic carbon sink (IC-Sink) and the pyrogenic carbon sink (PyC-Sink). The deviation of the measured from the expected C-Sinks and IC-Sinks is expressed as percentage. The deviation of the measured from expected geogenic IC-Sink refers to the IC-Sink solely occurring from mineral weathering (calculated after equations 9-12, supplementary information S6).), while fluxes of K^{+} are mainly contributed by biochar alone. Taken together, these patterns show that biochar acts not only as an additional carbon source but also as an

743 interactive modifier of mineral weathering by altering cation mobility, sorption processes, DSi
744 retention, and solution chemistry, while the mineral determines which cations are available
745 for release and which secondary phases may form.

746 In general, the co-application with biochar has a remarkable effect on DOC leaching (Figure 3,
747 supplementary information S11). DOC leaching with peridotite, basanite and steel slag is
748 disproportionally reduced compared to expected values and the DOC retention from concrete
749 is not fully counterbalanced by the biochar DOC leaching. These results highlight the
750 importance of organo-mineral interactions in reducing SOC losses and likely promoting MAOM
751 formation (Buss et al., 2024, 2023; Xu et al., 2024). Except for steel slag, the combined CO_2
752 drawdown remaining from the IC-Sink and DOC retention is higher for the co-applications than
753 for their corresponding single application. The addition of biochar can be seen as an effective
754 measure to counterbalance SOC loss under ERW as already shown in modelling studies
755 (Maslouski et al., 2025). Regarding trace metal leaching, co-applications of biochar with
756 peridotite and steel slag exceeds net nickel concentrations of the German Drinking Water
757 Ordinance. Co-applications with silicate minerals also exceed lead concentrations, which is
758 mainly attributed to the high lead leaching from biochar, while the leaching of lead from
759 industrial materials is reduced. We assume that high Ca^{2+} fluxes may support the precipitation
760 of $PbCO_3$ in co-precipitation with $CaCO_3$ (Saleh et al., 2026). Nonetheless, 60% of the
761 co-applications exhibited net trace metal retention (Table 4), demonstrating that this
762 approach still provides a mitigating effect despite these critical cases. Our results on the co-
763 application indicate that biochar can support both mineral weathering and SOC preservation,
764 but its net effect depends on whether sorption, cation retention, or trace-metal mobilization
765 dominates under a given material combination.

766

767 ### 4.3.3 Co-pyrolysis of minerals and biomass

768 In co-pyrolysis, the relevant mechanisms differ from co-application because minerals are
769 exposed to thermal treatment and can be transformed, eventually encapsulated, or activated
770 before soil deployment. Chemical fluxes of RE-biochars produced from dry-mixed and
771 wet-impregnated with concrete, steel slag, and basanite largely follow flux behaviour
772 observed in co-applications (Figure 3). Given their higher mineral content (62.1-67.4 wt%),
773 geogenic IC-Sinks are expected to be higher than in co-applications. However, for industrial
774 materials, geogenic IC-Sinks are 25–63% below their expected values, indicating suppressed

mineral weathering (Table 6). This pattern is consistent with the idea that minerals might undergo partial encapsulation within the biochar matrix during pyrolysis (Meyer zu Drewer et al., 2025) or limited dissolution due to a reduction of the mineral surface area from pyrolysis or from pellet compaction. Another reason could be the impact of pyrolysis temperature on the properties of the carbonate minerals within the industrial materials. Although not detected in the XRD measurements, hydrocarbonates may be present in the non-heated minerals as amorphous minerals (supplementary data D2). When heated to 650 °C, hydrocarbonates undergo complete decomposition, resulting in lower weathering rates (Coenen et al., 2016). In RE-biochars, the basanite K^+ fluxes mainly stem from biochar (Figure 3, supplementary data D7). The K^+ fluxes are lower proportional to the biochar content and may suggest a stabilizing effect from co-pyrolysis. The fluxes of all four major cations are generally higher in the basanite RE-biochar with wet-impregnation, suggesting benefits from suspension of the basanite powder. Together, these observations indicate that co-pyrolysis can either suppress or maintain mineral reactivity depending on how pyrolysis impacts mineral alteration, mineral surface accessibility and cation release from the matrix.

In peridotite RE-biochars, Mg^{2+} and DSi release is strongly enhanced (Figure 3). Given that peridotite contains 19.6% serpentine, pyrolysis likely induced thermal activation, consistent with transformations into metaserpentine and forsterite (Du Breuil et al., 2019). This provides a mechanistic explanation for why peridotite behaves differently from all other materials: instead of suppressing weathering, pyrolysis appears to increase the reactivity of the Mg-bearing phase. Mg^{2+} leaching increased by 170-175% and remained elevated (2.8x) through week 75, demonstrating long-lasting activation effects by co-pyrolysis. Similar long-term responses have been observed in other thermal activation studies with serpentine-rich rocks (Vorrath et al., in prep.). Although the IC-$Sink_{pot}$ of peridotite does not change, accelerated weathering may reduce the time lag before alkalinity becomes detectable in high-CEC soils (Kanzaki et al., 2025). Despite increased DOC leaching from peridotite RE-biochars, the combined CO_2 drawdown from the IC-Sink and DOC exceeds that of unheated peridotite by a factor of three. Thus, peridotite represents an exceptional case in which co-pyrolysis increases mineral reactivity rather than shielding it, highlighting that the direction of thermal effects is determined by mineral structure and phase transformations.

Trace metal concentrations from all RE-biochars exceed Pb thresholds of the German Drinking Water Ordinance, and steel slag RE-biochars show elevated Cd, Ni, and Pb, likely due to

breakdown of metal-bearing phases during pyrolysis. In contrast, peridotite RE-biochars exhibit lower Ni leaching than untreated peridotite (Table 4, supplementary information S7), increasing its potential application by enhanced trace metal retention for the mineral with the highest risk of nickel contamination in this study. Overall, co-pyrolysis should therefore be viewed as a mineral-specific thermal treatment that may either reduce or amplify trace metal release.

4.4 Distribution pathways of released cations

Our accounting of cations in the exchangeable fraction of post-experiment soils shows that cation concentrations in the leachate water are 3 to 54 times higher (Table 5). For nearly all amendments, the exchangeable fraction represents only a small proportion of total cation release, with a maximum of 2.1% of the input material. This pattern likely reflects the low CEC and low TOC of the sandy soil that did not change in the control over the term of 75 weeks, as well as the absence of plants or soil fauna. In contrast, pot experiments with soils of higher CEC show the opposite trend, where most cations are retained in exchangeable fractions, carbonates, (hydr)oxides, or SOM-associated pools, with little or no leaching observed (Boito et al., 2025; Niron et al., 2024; Steinwidder et al., 2026; Te Pas et al., 2026; Vienne et al., 2026b, 2024). This supports the view of Bijma et al. (2026) that robust CDR accounting requires tracking cations across all soil pools, not only in the leachate.

Both relative and absolute cation values (Table 5, supplementary data D9) reveal higher proportions of divalent cations (Ca^{2+}, Mg^{2+}) in the exchangeable fraction compared to monovalent cations (K^{+}, Na^{+}), except for Ca^{2+} with all peridotite amendments and pure biochar. Ca^{2+} retention in basanite amendments, indicated by negative values in the leachate water or positive values in the exchangeable fraction, shows that divalent cations first pass through the exchangeable pool before contributing to the IC-Sink in the leachate. For peridotite amendments, negative values in both exchangeable and leachate fraction point toward redistribution of Ca^{2+} into other soil pools. Exchangeable Ca^{2+} saturation after the experiment is highest in soils receiving carbonate amendments (0.9 mmol for concrete and limestone) and near zero to negative for silicates (-0.9 mmol for peridotite), consistent with higher Ca^{2+} fluxes as seen in other studies (Hammes et al., 2025). Similar increases in Ca^{2+} saturation during steel slag weathering were also observed by Maxbauer et al. (2026), supporting a proportional relationship between Ca^{2+} saturation and Ca^{2+} release.

Although other soil cation pools were not measured, several interactions likely may have influenced Ca^{2+} and Mg^{2+} mobility. Many studies suggest that part of the released cations becomes incorporated into secondary minerals within weeks to months (Dietzen and Rosing, 2023; Hammes et al., 2025; Niron et al., 2024; Steinwidder et al., 2026; Te Pas et al., 2026, 2025), and that secondary precipitation may occur even from undersaturated solutions (Ruiz-Agudo et al., 2012). Fast-weathering minerals tend to produce more secondary precipitates, while slowly weathering phases reduce cation incorporation, potentially enhancing CDR by minimizing precipitation losses (Steinwidder et al., 2026). In our experiment, only small decreases in inorganic carbon were detected (supplementary data D10), making significant carbonate precipitation unlikely. Amorphous and crystalline phases, including aluminosilicate clays and (hydr)oxides, may serve as sinks for Ca^{2+} and Mg^{2+}, consistent with evidence of Ca^{2+}- and Mg^{2+}-bearing secondary minerals such as kaolinite and 2:1 layer silicates (Steinwidder et al., 2026; Te Pas et al., 2026). Interactions of Ca^{2+} and Mg^{2+} with soil organic matter may also contribute to MAOM formation (Buss et al., 2023; Vienne et al., 2026a), potentially supported by iron (hydr)oxide formation, which is known to stabilize SOC over the long term (Kleber et al., 2015; Te Pas et al., 2026). Although SOC stocks increased slightly in most amendments and most changes in CEC could be associated with cation fluxes from the input material, these results must be interpreted with caution, as fine biochar particles may have contributed to measured SOC despite careful sampling.

Monovalent cations (K^+, Na^+) show higher variability in both exchangeable and leachate fractions, sometimes exceeding their input amounts in treatments with concrete, steel slag, peridotite, and biochar. Na^+ may originate from dissolution of in-situ feldspar and feldspathoid minerals or from exchange with other cations due to preferential adsorption order (Tan, 2010), resulting in additional export. Na^+ also serves as a clear indicator of basanite weathering (Dupla et al., 2025), and is mostly exported in the leachate. Elevated K^+ fluxes likely reflect the release of soil-inherent K^+ due to cation exchange processes as well. In agricultural settings, plants could access additional K^+ from the soil beyond amendment inputs (Swoboda et al., 2022), though this effect is absent in our plant-free setup.

Overall, all amendments show net release of major cations, except for Ca^{2+} and Na^+ in peridotite and Ca^{2+} for basanite amendments. Because we did not measure all soil cation pools (e.g., mineral-associated organic matter, oxide-bound pools), precise weathering quantification is not possible. Nevertheless, the combined cation release from exchangeable

fractions and leachate provides a conservative lower-bound estimate of weathering intensity and exported alkalinity, especially given the soil's low clay and carbonate content. Based on this combined accounting, dissolution over 75 weeks is at least 6.8% for concrete, 5.8% for steel slag, and lower for limestone (4.0%), basanite (4.1%), and peridotite (1.4%) (supplementary data D9).

5 Conclusion

Our study demonstrates that ERW-biochar interactions in soil systems produce distinct and material-specific impacts on C_{org} conversion, mineral weathering, and the formation of both inorganic and organic C-Sinks. The effects of combining biochar and minerals are non-additive and depend strongly on the specific amendment combination. In co-applications, biochar may modify water drainage and soil solution chemistry through cation retention and sorption and thereby sustain mineral weathering, whereas in RE-biochars minerals may be embedded in the biochar matrix, so pyrolysis may either suppress weathering by reducing mineral surface exposure. For serpentine-rich materials, co-pyrolysis can increase reactivity and weathering through thermal activation. These impacts are time dependent, with early fast-release processes, intermediate stabilisation, and later redistribution among soil pools jointly shaping the observed fluxes. They reflect a common process framework involving mineral dissolution, cation exchange, sorption to biochar surfaces, secondary mineral formation, and, in the case of co-pyrolysis, thermal alteration of mineral phases, but the relative importance of these processes varies strongly among materials. Co-pyrolysis can further enhance carbon retention in biochar, particularly with wet-impregnation of Mg^{2+} ions, but often suppresses carbonate weathering, thereby reducing the geogenic IC-Sink. In contrast, co-application of minerals and biochar consistently improves weathering conditions, accelerate the development of the geogenic IC-Sinks for most minerals, and reduces DOC losses, making it an effective and practical strategy for combined CDR approaches under the sandy soil conditions tested here. Overall, the combined C-Sink emerges from interacting processes rather than from a simple sum of individual amendment effects.

Among pure mineral amendments, concrete and limestone facilitate DOC retention and achieve moderate IC-Sink efficiencies, whereas silicates such as basanite and peridotite contribute more modestly but steadily to long-term alkalinity production. Thermal activation

of peridotite through co-pyrolysis remarkably accelerates Mg^{2+} release and inhibits Ni release, highlighting the potential of heat-induced mineral transformations to shorten weathering time lags. However, the benefits of accelerated dissolution must be weighed against increased trace metal mobility and reduced C-Sink performance in RE-biochars derived from industrial materials. As a result, the direction of the combined effect is governed by mineral-specific properties, including mineral composition and susceptibility to thermal alteration.

The distribution of released cations shows that in coarse-textured, low-CEC soils, most cations are exported through leaching rather than retained in exchangeable fractions, allowing leachate fluxes to serve as conservative lower-bound estimates of weathering. Further, the nearly complete release of the biogenic IC-Sink allowed to quantify the contributions of the mineral-derived geogenic IC-Sink to the total C-Sink. Secondary mineral formation likely accounts for part of the missing cation mass balance, underscoring the need for more comprehensive measurements of mineral-associated organic matter, (hydr)oxide pools, and amorphous phases in future experiments.Overall, our findings indicate that co-application of mineral powders and biochar offers the best balance between C-Sink formation, weathering enhancement, trace-metal safety, and operational feasibility. RE-biochars may provide targeted benefits, such as improved carbon stability, increased C_{org} conversion into biochar or accelerated silicate dissolution, but they do not consistently outperform simpler deployment strategies. For field implementation, site-specific soil properties, mineral composition, regulatory thresholds for trace metals, and broader logistical considerations must be carefully integrated into amendment selections and MRV frameworks. Our results highlight the need for long-term field studies and multi-pool carbon accounting to fully capture mineral-organic interactions and optimise combined ERW-biochar strategies for durable carbon removal, while also covering material-specific responses, indicating that no single universal interaction pathway can explain all amendment combinations studied here.

Acknowledgements

We warmly want to thank our lab technicians Peggy Bartsch and Tom Jäppinen and our student assistant Irmak Gök. We also thank Peter Stutz and Stefan Jung from the University of Hamburg for XRF measurements, Sebastian Lindhorst from the University of Hamburg for grain size distribution measurements, José Maria de la Rosa from the Institute of Natural

Resources and Agrobiology of Sevilla for TGA measurements, William Meredith from the University of Nottingham for hydropyrolysis analyses, the team from the Element Analysis, Chemistry Department, University Hamburg for the trace metal analyses, and Sören Beckmann for logistical support at the Geomatikum, University of Hamburg.

We also like to thank for the trust and the support from Caspar von Ziegner, Esther Jäckel, Jens Heberling and Lars Macketanz from Novocarbo, Michael Dohlen from Thyssenkrupp AG, Maurice Bryson from Silicate Carbon Limited and Andrew Simeonidis from Sibelco. We also thank Nikolas Hagemann from the Ithaka Institute for Carbon Strategies, Germany.

Author contributions

MEV conceptualized and coordinated the research project and acquired the funding, designed the study, prepared visualizations and wrote the original manuscript. MEV, JMD, CA, LS, LF, SN, IN performed the experiments. MEV and JMD analysed the data. MS and TS assisted with the pellet press, DE provided AAS measurements for trace metals. JH supported with the institutional framework. All authors contributed to the discussion and manuscript writing and provided valuable input.

Funding Sources

The project proudly received funding as “The Rockchar Project” from the Klaus Tschira Boost Fund, a joint initiative of GSO – Guidance, Skills & Opportunities for Researchers e.V. and the Klaus Tschira Stiftung.

References

Amann, T., Hartmann, J., 2019. Ideas and perspectives: Synergies from co-deployment of negative emission technologies. Biogeosciences 16, 2949–2960. https://doi.org/10.5194/bg-16-2949-2019

Amann, T., Hartmann, J., Hellmann, R., Pedrosa, E.T., Malik, A., 2022. Enhanced weathering potentials—the role of in situ CO2 and grain size distribution. Front. Clim. 4, 929268. https://doi.org/10.3389/fclim.2022.929268

Amann, T., Hartmann, J., Struyf, E., De Oliveira Garcia, W., Fischer, E.K., Janssens, I., Meire, P., Schoelynck, J., 2020. Enhanced Weathering and related element fluxes – a cropland mesocosm approach. Biogeosciences 17, 103–119. https://doi.org/10.5194/bg-17-103-2020

Ansari, M., Lübeck, A., Meyer zu Drewer, J., Hagemann, N., Eschenbach, A., Becker, J.N., in review. Rock-enhanced biochar has similar priming effect as pure biochar application, but improves short-term carbon stabilization in agricultural soils. Biology and Fertility of Soils.

Ansari, M., Stock, S., Dippold, M.A., Hamburger, S.E., Kammann, C.I., Meyer Zu Drewer, J., Hagemann, N., Eschenbach, A., Becker, J.N., 2026. Biochar dominated the combined effect of silicate rock powder and biochar application on extracellular enzyme kinetics and nutrient dynamics in a sandy soil. Soil and Tillage Research 262, 107234. https://doi.org/10.1016/j.still.2026.107234

Anthony, T.L., Jones, A.R., Silver, W.L., 2025. Supplementing Enhanced Weathering With Organic Amendments Accelerates the Net Climate Benefit of Soil Amendments in Rangeland Soils. AGU Advances 6, e2024AV001480. https://doi.org/10.1029/2024AV001480

Azzi, E.S., Li, H., Cederlund, H., Karltun, E., Sundberg, C., 2024. Modelling biochar long-term carbon storage in soil with harmonized analysis of decomposition data. Geoderma 441, 116761. https://doi.org/10.1016/j.geoderma.2023.116761

Babiker, M., Berndes, G., Blok, K., Cohen, B., Cowie, A., Geden, O., Ginzburg, V., Leip, A., Smith, P., Sugiyama, M., Yamba, F., 2022. Cross-sectoral perspectives, in: Shukla, P.R., Skea, J., Slade, R., Al Khourdajie, A., van Diemen, R., McCollum, D., Pathak, M., Some, S., Vyas, P., Fradera, R., Belkacemi, M., Hasija, A., Lisboa, G., Luz, S., Malley, J. (Eds.), Climate Change 2022: Mitigation of Climate Change. Contribution of Working Group III to the Sixth Assessment Report of the Intergovernmental Panel on Climate Change. Cambridge University Press, Cambridge, UK and New York, NY, USA, pp. 1245–1354. https://doi.org/10.1017/9781009157926.014

Bang, J., Hesterberg, D., 2004. Dissolution of trace element contaminants from two coastal plain soils as affected by pH. J Environ Qual 33, 891–901. https://doi.org/10.2134/jeq2004.0891

Beerling, D.J., Leake, J.R., Long, S.P., Scholes, J.D., Ton, J., Nelson, P.N., Bird, M., Kantzas, E., Taylor, L.L., Sarkar, B., Kelland, M., DeLucia, E., Kantola, I., Müller, C., Rau, G., Hansen, J., 2018. Farming with crops and rocks to address global climate, food and soil security. Nature Plants 4, 138–147. https://doi.org/10.1038/s41477-018-0108-y

Bijma, J., Hagens, M., Hammes, J.S., Planavsky, N., Pogge Von Strandmann, P.A.E., Reershemius, T., Reinhard, C.T., Renforth, P., Suhrhoff, T.J., Vicca, S., Vienne, A., Wolf-Gladrow, D., 2026. Reviews and syntheses: Carbon vs. cation based MRV of Enhanced Rock Weathering and the issue of soil organic carbon. Biogeosciences 23, 53–75. https://doi.org/10.5194/bg-23-53-2026

Boito, L., Steinwidder, L., Rijnders, J., Berwouts, J., Janse, S., Niron, H., Roussard, J., Vienne, A., Vicca, S., 2025. Enhanced Rock Weathering Altered Soil Organic Carbon Fluxes in a Plant Trial. Global Change Biology 31, e70373. https://doi.org/10.1111/gcb.70373

Borchard, N., Schirrmann, M., Cayuela, M.L., Kammann, C., Wrage-Mönnig, N., Estavillo, J.M., Fuertes-Mendizábal, T., Sigua, G., Spokas, K., Ippolito, J.A., Novak, J., 2019. Biochar, soil and land-use interactions that reduce nitrate leaching and N2O emissions: A meta-analysis. Science of The Total Environment 651, 2354–2364. https://doi.org/10.1016/j.scitotenv.2018.10.060

Buckingham, F.L., Henderson, G.M., 2024. The enhanced weathering potential of a range of silicate and carbonate additions in a UK agricultural soil. Science of The Total Environment 907, 167701. https://doi.org/10.1016/j.scitotenv.2023.167701

Buss, W., Hasemer, H., Ferguson, S., Borevitz, J., 2023. Stabilisation of soil organic matter with rock dust partially counteracted by plants. Global Change Biology 30, e17052. https://doi.org/10.1111/gcb.17052

Buss, W., Hasemer, H., Sokol, N.W., Rohling, E.J., Borevitz, J., 2024. Applying minerals to soil to draw down atmospheric carbon dioxide through synergistic organic and inorganic pathways. Commun Earth Environ 5, 602. https://doi.org/10.1038/s43247-024-01771-3

Buss, W., Jansson, S., Wurzer, C., Mašek, O., 2019. Synergies between BECCS and Biochar—Maximizing Carbon Sequestration Potential by Recycling Wood Ash. ACS Sustainable Chem. Eng. 7, 4204–4209. https://doi.org/10.1021/acssuschemeng.8b05871

Buss, W., Wurzer, C., Manning, D.A.C., Rohling, E.J., Borevitz, J., Mašek, O., 2022. Mineral-enriched biochar delivers enhanced nutrient recovery and carbon dioxide removal. Commun Earth Environ 3, 67. https://doi.org/10.1038/s43247-022-00394-w

Camino-Serrano, M., Graf Pannatier, E., Vicca, S., Luyssaert, S., Jonard, M., Ciais, P., Guenet, B., Gielen, B., Peñuelas, J., Sardans, J., Waldner, P., Etzold, S., Cecchini, G., Clarke, N., Galić, Z., Gandois, L., Hansen, K., Johnson, J., Klinck, U., Lachmanová, Z., Lindroos, A.-J., Meesenburg, H., Nieminen, T.M., Sanders, T.G.M., Sawicka, K., Seidling, W., Thimonier, A., Vanguelova, E., Verstraeten, A., Vesterdal, L., Janssens, I.A., 2016. Trends in soil solution dissolved organic carbon (DOC) concentrations acrossEuropean forests. Biogeosciences 13, 5567–5585. https://doi.org/10.5194/bg-13-5567-2016

Chiaravalloti, I., Zhang, S., Planavsky, N., 2025. Assessing CO2 fluxes during enhanced weathering from soils through a mesocosm lens. CDRXIV.

Cipolla, G., Calabrese, S., Porporato, A., Noto, L.V., 2022. Effects of precipitation seasonality, irrigation, vegetation cycle and soil type on enhanced weathering – modeling of cropland case studies across four sites. Biogeosciences 19, 3877–3896. https://doi.org/10.5194/bg-19-3877-2022

Coenen, K., Gallucci, F., Cobden, P., van Dijk, E., Hensen, E., van Sint Annaland, M., 2016. Chemisorption working capacity and kinetics of CO2 and H2O of hydrotalcite-based adsorbents for sorption-enhanced water-gas-shift applications. Chemical Engineering Journal 293, 9–23. https://doi.org/10.1016/j.cej.2016.02.050

Cornelissen, G., Briels, N., Bucheli, T.D., Estoppey, N., Gredelj, A., Hagemann, N., Lerch, S., Lotz, S., Rasse, D., Schmidt, H.-P., Sørmo, E., Arp, H.P.H., 2025. A Virtuous Cycle of Phytoremediation, Pyrolysis, and Biochar Applications toward Safe PFAS Levels in Soil, Feed, and Food. J. Agric. Food Chem. 73, 3283–3285. https://doi.org/10.1021/acs.jafc.5c00651

Deng, H., Sonnenthal, E., Arora, B., Breunig, H., Brodie, E., Kleber, M., Spycher, N., Nico, P., 2023. The environmental controls on efficiency of enhanced rock weathering in soils. Sci Rep 13, 9765. https://doi.org/10.1038/s41598-023-36113-4

Dickson, A.G., 1981. An exact definition of total alkalinity and a procedure for the estimation of alkalinity and total inorganic carbon from titration data. Deep Sea Research Part A. Oceanographic Research Papers 28, 609–623. https://doi.org/10.1016/0198-0149(81)90121-7

Dietzen, C., Rosing, M.T., 2023. Quantification of CO2 uptake by enhanced weathering of silicate minerals applied to acidic soils. International Journal of Greenhouse Gas Control 125, 103872. https://doi.org/10.1016/j.ijggc.2023.103872

Ding, Y., Liu, Y.-X., Wu, W.-X., Shi, D.-Z., Yang, M., Zhong, Z.-K., 2010. Evaluation of Biochar Effects on Nitrogen Retention and Leaching in Multi-Layered Soil Columns. Water Air Soil Pollut 213, 47–55. https://doi.org/10.1007/s11270-010-0366-4

Du Breuil, C., César-Pasquier, L., Dipple, G., Blais, J.-F., Iliuta, M., Mercier, G., 2019. Mineralogical Transformations of Heated Serpentine and Their Impact on Dissolution during Aqueous-Phase Mineral Carbonation Reaction in Flue Gas Conditions. Minerals 9, 680. https://doi.org/10.3390/min9110680

Dupla, X., Bertagni, M.B., Grand, S., 2025. Three Years of Field Trials Indicate a Sustained Enhanced Rock Weathering Signal with Limited CO2 Removal. Environ. Sci. Technol. 59, 25751–25764. https://doi.org/10.1021/acs.est.5c09820

Dupla, X., Claustre, R., Bonvin, E., Graf, I., Le Bayon, R.-C., Grand, S., 2024. Let the dust settle: Impact of enhanced rock weathering on soil biological, physical, and geochemical fertility. Science of The Total Environment 954, 176297. https://doi.org/10.1016/j.scitotenv.2024.176297

EBC, 2024. Guidelines for a Sustatinable Production of Biochar (No. Version 10.4G). Ithaka Institute, Arbaz, Switzerland.

Fang, Q., Lu, A., Hong, H., Kuzyakov, Y., Algeo, T.J., Zhao, L., Olshansky, Y., Moravec, B., Barrientes, D.M., Chorover, J., 2023. Mineral weathering is linked to microbial priming in the critical zone. Nat Commun 14, 345. https://doi.org/10.1038/s41467-022-35671-x

Gao, H., Weng, L., Comans, R.N.J., Koopmans, G.F., 2025. Dual-Domain Regulation of Dissolved Organic Matter Release in Soil: The Role of pH and Calcium. ACS Earth Space Chem. 9, 1377–1391. https://doi.org/10.1021/acsearthspacechem.4c00377

Grafmüller, J., Böhm, A., Zhuang, Y., Spahr, S., Müller, P., Otto, T.N., Bucheli, T.D., Leifeld, J., Giger, R., Tobler, M., Schmidt, H.-P., Dahmen, N., Hagemann, N., 2022. Wood Ash as an Additive in Biomass Pyrolysis: Effects on Biochar Yield, Properties, and Agricultural Performance. ACS Sustainable Chem. Eng. 10, 2720–2729. https://doi.org/10.1021/acssuschemeng.1c07694

Hagemann, N., Schmidt, H.-P., Bucheli, T.D., Grafmüller, J., Vosswinkel, S., Herdegen, V., Meredith, W., Uguna, C.N., Snape, C.E., 2025. Proxies for use in biochar decay models: Hydropyrolysis, electric conductivity, and H/Corg molar ratio. PLoS One 20, e0330206. https://doi.org/10.1371/journal.pone.0330206

Hammes, J.S., Hartmann, J., Barth, J.A.C., Linke, T., Smet, I., Hagens, M., Pogge Von Strandmann, P.A.E., Reershemius, T., Casimiro, B., Vienne, A., Stoeckel, A.A., Steffens, R., Paessler, D., 2025. Soil processes govern alkalinity and cation retention in enhanced weathering for carbon dioxide removal. https://doi.org/10.5194/egusphere-2025-5402

Han, L., Sun, K., Yang, Y., Xia, X., Li, F., Yang, Z., Xing, B., 2020. Biochar's stability and effect on the content, composition and turnover of soil organic carbon. Geoderma 364, 114184. https://doi.org/10.1016/j.geoderma.2020.114184

Haque, F., Santos, R.M., Chiang, Y.W., 2020. Optimizing Inorganic Carbon Sequestration and Crop Yield With Wollastonite Soil Amendment in a Microplot Study. Frontiers in Plant Science 11.

Hartmann, J., West, A.J., Renforth, P., Köhler, P., De La Rocha, C.L., Wolf-Gladrow, D.A., Dürr, H.H., Scheffran, J., 2013. Enhanced chemical weathering as a geoengineering strategy to reduce atmospheric carbon dioxide, supply nutrients, and mitigate ocean acidification. Rev. Geophys. 51, 113–149. https://doi.org/10.1002/rog.20004

Heřmanská, M., Voigt, M.J., Marieni, C., Declercq, J., Oelkers, E.H., 2023. A comprehensive and consistent mineral dissolution rate database: Part II: Secondary silicate minerals. Chemical Geology 636, 121632. https://doi.org/10.1016/j.chemgeo.2023.121632

Heřmanská, M., Voigt, M.J., Marieni, C., Declercq, J., Oelkers, E.H., 2022. A comprehensive and internally consistent mineral dissolution rate database: Part I: Primary silicate minerals and glasses. Chemical Geology 597, 120807. https://doi.org/10.1016/j.chemgeo.2022.120807

Hong, H., Churchman, G.J., Yin, K., Li, R., Li, Z., 2014. Randomly interstratified illite–vermiculite from weathering of illite in red earth sediments in Xuancheng, southeastern China. Geoderma 214–215, 42–49. https://doi.org/10.1016/j.geoderma.2013.10.004

Honvault, N., Tiouchichine, M.-L., Sauze, J., Piel, C., Landais, D., Devidal, S., Gritti, E., Bosch, D., Milcu, A., 2024. Additive effects of basalt enhanced weathering and biochar co-application on carbon sequestration, soil nutrient status and plant performance in a mesocosm experiment. Applied Geochemistry 169, 106054. https://doi.org/10.1016/j.apgeochem.2024.106054

Ippolito, J.A., Cui, L., Kammann, C., Wrage-Mönnig, N., Estavillo, J.M., Fuertes-Mendizabal, T., Cayuela, M.L., Sigua, G., Novak, J., Spokas, K., Borchard, N., 2020. Feedstock choice, pyrolysis temperature and type influence biochar characteristics: a comprehensive meta-data analysis review. Biochar 2, 421–438. https://doi.org/10.1007/s42773-020-00067-x

Isometric, 2025. Enhanced Weathering in Agriculture v1.1. https://doi.org/https://registry.isometric.com/protocol/enhanced-weathering-agriculture/enhanced-weathering-agriculture/1.1/1.1.2

Janssens, I.A., Roobroeck, D., Sardans, J., Obersteiner, M., Peñuelas, J., Richter, A., Smith, P., Verbruggen, E., Vicca, S., 2022. Negative erosion and negative emissions: Combining multiple land-based carbon dioxide removal techniques to rebuild fertile topsoils and enhance food production. Front. Clim. 4, 928403. https://doi.org/10.3389/fclim.2022.928403

Jiang, Y., Zhou, L., Zhu, Z., Ma, L., Chen, J., Li, Y., 2022. Research on dynamic cracking properties of cracked rock mass under the effect of thermal treatment. Theoretical and Applied Fracture Mechanics 122, 103580. https://doi.org/10.1016/j.tafmec.2022.103580

Kalbitz, K., Solinger, S., Park, J.-H., Michalzik, B., Matzner, E., 2000. CONTROLS ON THE DYNAMICS OF DISSOLVED ORGANIC MATTER IN SOILS: A REVIEW. Soil Science 165, 277.

Kammann, C., Ratering, S., Eckhard, C., Müller, C., 2012. Biochar and Hydrochar Effects on Greenhouse Gas (Carbon Dioxide, Nitrous Oxide, and Methane) Fluxes from Soils. Journal of Environmental Quality 41, 1052–1066. https://doi.org/10.2134/jeq2011.0132

Kantola, I.B., Blanc-Betes, E., Masters, M.D., Chang, E., Marklein, A., Moore, C.E., Von Haden, A., Bernacchi, C.J., Wolf, A., Epihov, D.Z., Beerling, D.J., DeLucia, E.H., 2023. Improved net carbon budgets in the US Midwest through direct measured impacts of enhanced weathering. Global Change Biology 29, 7012–7028. https://doi.org/10.1111/gcb.16903

Kanzaki, Y., Planavsky, N.J., Zhang, S., Jordan, J., Suhrhoff, T.J., Reinhard, C.T., 2025. Soil cation storage is a key control on the carbon removal dynamics of enhanced weathering. Environ. Res. Lett. 20, 074055. https://doi.org/10.1088/1748-9326/ade0d5

Karr-Lilienthal, L.K., Grieshop, C.M., Merchen, N.R., Mahan, D.C., Fahey, G.C., 2004. Chemical Composition and Protein Quality Comparisons of Soybeans and Soybean Meals from Five Leading Soybean-Producing Countries. J. Agric. Food Chem. 52, 6193–6199. https://doi.org/10.1021/jf049795+

Keiluweit, M., Nico, P.S., Johnson, M.G., Kleber, M., 2010. Dynamic Molecular Structure of Plant Biomass-Derived Black Carbon (Biochar). Environ. Sci. Technol. 44, 1247–1253. https://doi.org/10.1021/es9031419

Kelemen, P.B., Matter, J., Streit, E.E., Rudge, J.F., Curry, W.B., Blusztajn, J., 2011. Rates and Mechanisms of Mineral Carbonation in Peridotite: Natural Processes and Recipes for Enhanced, in situ CO2 Capture and Storage. Annual Review of Earth and Planetary Sciences 39, 545–576. https://doi.org/10.1146/annurev-earth-092010-152509

Kitsopoulos, K.P., 1999. Cation-Exchange Capacity (CEC) of Zeolitic Volcaniclastic Materials: Applicability of the Ammonium Acetate Saturation (AMAS) Method. Clays and clay miner. 47, 688–696. https://doi.org/10.1346/CCMN.1999.0470602

Kleber, M., Eusterhues, K., Keiluweit, M., Mikutta, C., Mikutta, R., Nico, P.S., 2015. Mineral–Organic Associations: Formation, Properties, and Relevance in Soil Environments, in: Advances in Agronomy. Elsevier, pp. 1–140. https://doi.org/10.1016/bs.agron.2014.10.005

Lalitha, M., Parvathy, S., Koyal, A., Hegde, R., Ramamurthy, V., 2026. Impact of Calcium Carbonate Solubility on Estimating Soil Exchangeable Cations in Calcareous Soils Using 1N Ammonium Acetate Method. Communications in Soil Science and Plant Analysis 57, 480–490. https://doi.org/10.1080/00103624.2026.2617299

Lasaga, A.C., Berner, R.A., 1998. Fundamental aspects of quantitative models for geochemical cycles. Chemical Geology 145, 161–175. https://doi.org/10.1016/S0009-2541(97)00142-3

Lehmann, J., Cowie, A., Masiello, C.A., Kammann, C., Woolf, D., Amonette, J.E., Cayuela, M.L., Camps-Arbestain, M., Whitman, T., 2021. Biochar in climate change mitigation. Nat. Geosci. 14, 883–892. https://doi.org/10.1038/s41561-021-00852-8

Li, F., Cao, X., Zhao, L., Wang, J., Ding, Z., 2014. Effects of Mineral Additives on Biochar Formation: Carbon Retention, Stability, and Properties. Environ. Sci. Technol. 48, 11211–11217. https://doi.org/10.1021/es501885n

Li, L., Zhang, Y.-J., Novak, A., Yang, Y., Wang, J., 2021. Role of Biochar in Improving Sandy Soil Water Retention and Resilience to Drought. Water 13, 407. https://doi.org/10.3390/w13040407

Liu, D., Li, M., Yu, R., Li, H., Shen, Y., Tian, Q., Bu, H., Huang, C., Tan, W., 2023. Interlayer organic matter within hydroxy-interlayered clay minerals enhances soil organic carbon stability under long-term organic fertilization. Applied Clay Science 239, 106963. https://doi.org/10.1016/j.clay.2023.106963

Ma, Z., Yang, Y., Wu, Y., Xu, J., Peng, H., Liu, X., Zhang, W., Wang, S., 2019. In-depth comparison of the physicochemical characteristics of bio-char derived from biomass pseudo components: Hemicellulose, cellulose, and lignin. Journal of Analytical and Applied Pyrolysis 140, 195–204. https://doi.org/10.1016/j.jaap.2019.03.015

Mahanta, B., Singh, T.N., Ranjith, P.G., 2016. Influence of thermal treatment on mode I fracture toughness of certain Indian rocks. Engineering Geology 210, 103–114. https://doi.org/10.1016/j.enggeo.2016.06.008

Mašek, O., Buss, W., Brownsort, P., Rovere, M., Tagliaferro, A., Zhao, L., Cao, X., Xu, G., 2019. Potassium doping increases biochar carbon sequestration potential by 45%, facilitating decoupling of carbon sequestration from soil improvement. Sci Rep 9, 5514. https://doi.org/10.1038/s41598-019-41953-0

Maslouski, M., Ansari, M., Hamburger, S.E., Meyer Zu Drewer, J., Hagemann, N., Eschenbach, A., Beer, C., Becker, J.N., Kammann, C.I., Vorrath, M.-E., Porada, P., 2025. Long-term carbon dioxide removal potential from the application of wood biochar and basanite

rock powder in sandy soil using the LiDELSv2 process-based modeling approach. Environ. Res. Lett. 20, 124032. https://doi.org/10.1088/1748-9326/ae21f6

Maxbauer, D.P., Milliken, E., Yambing, J.R., Watson, E., Gregg, R.B., Swanson, L., Sohng, J., Sokol, N.W., Planavsky, N.J., 2026. Evidence for carbon dioxide removal via enhanced rock weathering with steel slag, though not basalt, in a midwestern U.S. field trial. Front. Clim. 7, 1657058. https://doi.org/10.3389/fclim.2025.1657058

Mbow, C., Rosenzweig, C., Barioni, L.G., Benton, T.G., Herrero, M., Krishnapillai, M., Liwenga, E., Pradhan, P., Rivera-Ferre, M.G., Sapkota, T., Tubiello, F.N., Xu, Y., 2022. Food Security, in: Shukla, P.R., Skea, J., Calvo Buendia, E., Masson-Delmotte, V., Pörtner, H.-O., Roberts, D.C., Zhai, P., Slade, R., Connors, S.L., van Diemen, R., Ferrat, M., Haughey, E., Luz, S., Neogi, S., Pathak, M., Petzold, J., Portugal-Pereira, J., Vyas, P., Huntley, E., Kissick, K., Belkacemi, M., Malley, J. (Eds.), Climate Change and Land: IPCC Special Report on Climate Change, Desertification, Land Degradation, Sustainable Land Management, Food Security, and Greenhouse Gas Fluxes in Terrestrial Ecosystems. Cambridge University Press. https://doi.org/10.1017/9781009157988

McDermott, F., Bryson, M., Magee, R., Van Acken, D., 2024. Enhanced weathering for CO2 removal using carbonate-rich crushed returned concrete; a pilot study from SE Ireland. Applied Geochemistry 169, 106056. https://doi.org/10.1016/j.apgeochem.2024.106056

Meredith, W., McBeath, A., Ascough, P., Bird, M.I., 2017. Analysis of biochars by hydropyrolysis (HyPy), in: Singh, B., Camps Arbestain, M., Lehmann, J. (Eds.), . CRC Press, Clayton.

Meyer zu Drewer, J., Vorrath, M.-E., Amann, T., Hartmann, J., Ansari, M., Cárcamo Perez, M., Hagemann, N., accepted. Combining biochar and basanite rock powder enhances carbon dioxide removal by carbonate alkalinity production. Frontiers in Climate.

Meyer zu Drewer, J., Vorrath, M.-E., Amann, T., Hartmann, J., De La Rosa, J.M., Möllmer, J., Pérez-Dalí, S.M., Meredith, W., Uguna, C., Snape, C., Kammann, C., Schmidt, H.-P., Hagemann, N., 2025. Pyrogenic carbon and carbonating minerals for carbon capture and storage (PyMiCCS) part I: production, physico-chemical characterization and C-sink potential. Front. Clim. 7. https://doi.org/10.3389/fclim.2025.1631368

Multer Hopkins, B., Lal, R., Lyons, W.B., Welch, S.A., 2024. Carbon capture potential and environmental impact of concrete weathering in soil. Science of The Total Environment 957, 177692. https://doi.org/10.1016/j.scitotenv.2024.177692

Nabuurs, G.-J., Mrabet, R., Abu Hatab, A., Bustamante, M., Clark, H., Havlík, P., House, J.I., Mbow, C., Ninan, K.N., Popp, A., Roe, S., Sohngen, B., Towprayoon, S., 2022. Agriculture, Forestry and Other Land Uses (AFOLU), in: Shukla, P.R., Skea, J., Slade, R., Al Khourdajie, A., van Diemen, R., McCollum, D., Pathak, M., Some, S., Vyas, P., Fradera, R., Belkacemi, M., Hasija, A., Lisboa, G., Luz, S., Malley, J. (Eds.), Climate Change 2022: Mitigation of Climate Change. Contribution of Working Group III to the Sixth Assessment Report of the Intergovernmental Panel on Climate Change. Cambridge University Press, Cambridge, UK and New York, NY, USA, pp. 747–860. https://doi.org/10.1017/9781009157926.009

Nan, H., Mašek, O., Yang, F., Xu, X., Qiu, H., Cao, X., Zhao, L., 2022. Minerals: A missing role for enhanced biochar carbon sequestration from the thermal conversion of biomass to the application in soil. Earth-Science Reviews 234, 104215. https://doi.org/10.1016/j.earscirev.2022.104215

Nan, H., Zhao, L., Yang, F., Liu, Y., Xiao, Z., Cao, X., Qiu, H., 2020. Different alkaline minerals interacted with biomass carbon during pyrolysis: Which one improved biochar carbon

sequestration? Journal of Cleaner Production 255, 120162. https://doi.org/10.1016/j.jclepro.2020.120162
Nieuwenhuize, J., Maas, Y.E.M., Middelburg, J.J., 1994. Rapid analysis of organic carbon and nitrogen in particulate materials. Marine Chemistry 45, 217–224. https://doi.org/10.1016/0304-4203(94)90005-1
Niron, H., Vienne, A., Frings, P., Poetra, R., Vicca, S., 2024. Exploring the synergy of enhanced weathering and *Bacillus subtilis* : A promising strategy for sustainable agriculture. Global Change Biology 30, e17511. https://doi.org/10.1111/gcb.17511
Oelkers, E.H., Declercq, J., Saldi, G.D., Gislason, S.R., Schott, J., 2018. Olivine dissolution rates: A critical review. Chemical Geology 500, 1–19. https://doi.org/10.1016/j.chemgeo.2018.10.008
Omara, P., Singh, H., Singh, K., Sharma, L., Otim, F., Obia, A., 2023. Short-term effect of field application of biochar on cation exchange capacity, pH, and electrical conductivity of sandy and clay loam temperate soils. TIA 3, 0–0. https://doi.org/10.48130/TIA-2023-0016
Palansooriya, K.N., Wong, J.T.F., Hashimoto, Y., Huang, L., Rinklebe, J., Chang, S.X., Bolan, N., Wang, H., Ok, Y.S., 2019. Response of microbial communities to biochar-amended soils: a critical review. Biochar 1, 3–22. https://doi.org/10.1007/s42773-019-00009-2
Parkhurst, D.L., Appelo, C.A.J., 2013. Description of input and examples for PHREEQC version 3—A computer program for speciation, batch-reaction, one-dimensional transport, and inverse geochemical calculations, in: U.S. Geological Survey Techniques and Methods. U.S. Geological Survey, Denver, p. 497.
Peng, X., Deng, Y., Peng, Y., Yue, K., 2018. Effects of biochar addition on toxic element concentrations in plants: A meta-analysis. Science of The Total Environment 616–617, 970–977. https://doi.org/10.1016/j.scitotenv.2017.10.222
Pignatello, J.J., Uchimiya, M., Abiven, S., 2024. Aging of biochar in soils and its implications, in: Biochar for Environmental Management. Routledge.
Planavsky, N.J., Ahmed, A.A., Suhrhoff, T.J., Reinhard, C.T., 2024. Cation uptake by biochar reduces carbon removal efficiency.
Rainbow, 2025. Enhanced rock weathering 1.0. https://doi.org/https://docs.rainbowstandard.io/methodologies/enhanced-rock-weathering
Renforth, P., 2019. The negative emission potential of alkaline materials. Nat Commun 10, 1401. https://doi.org/10.1038/s41467-019-09475-5
Rieder, L., Hagens, M., Poetra, R., Vidal, A., Calogiuri, T., Neubeck, A., Singh, A., Corbett, T., Niron, H., Vicca, S., Vlaeminck, S.E., Janssens, Iris, Verdonck, T., Janssens, Ivan, Li, X., Hammes, J.S., Hartmann, J., 2026. Contribution of dissolved organic carbon to total alkalinity in Enhanced Weathering experiments. Applied Geochemistry 198, 106685. https://doi.org/10.1016/j.apgeochem.2026.106685
Rijnders, J., Vicca, S., Struyf, E., Amann, T., Hartmann, J., Meire, P., Janssens, I., Schoelynck, J., 2023. The effects of dunite fertilization on growth and elemental composition of barley and wheat differ with dunite grain size and rainfall regimes. Front. Environ. Sci. 11, 1172621. https://doi.org/10.3389/fenvs.2023.1172621
Rijnders, J., Vienne, A., Vicca, S., 2025. Effects of basalt, concrete fines, and steel slag on maize growth and toxic trace element accumulation in an enhanced weathering experiment. Biogeosciences 22, 2803–2829. https://doi.org/10.5194/bg-22-2803-2025
Rinder, T., von Hagke, C., 2021. The influence of particle size on the potential of enhanced basalt weathering for carbon dioxide removal - Insights from a regional assessment.

Journal of Cleaner Production 315, 128178. https://doi.org/10.1016/j.jclepro.2021.128178
Rowley, M.C., Grand, S., Verrecchia, É.P., 2018. Calcium-mediated stabilisation of soil organic carbon. Biogeochemistry 137, 27–49. https://doi.org/10.1007/s10533-017-0410-1
Rueda, O., Mogollón, J.M., Tukker, A., Scherer, L., 2021. Negative-emissions technology portfolios to meet the 1.5 °C target. Global Environmental Change 67, 102238. https://doi.org/10.1016/j.gloenvcha.2021.102238
Ruiz-Agudo, E., Putnis, C.V., Rodriguez-Navarro, C., Putnis, A., 2012. Mechanism of leached layer formation during chemical weathering of silicate minerals. Geology 40, 947–950. https://doi.org/10.1130/G33339.1
Saleh, H., Braida, W., Zhang, Z., Datta, R., Sarkar, D., 2026. Geochemical fate of lead in contaminated residential soils following application of amendments for lead immobilization. Front Chem 14, 1742013. https://doi.org/10.3389/fchem.2026.1742013
Sanei, H., Petersen, H.I., Chiaramonti, D., Masek, O., 2025. Evaluating the two-pool decay model for biochar carbon permanence. Biochar 7, 9. https://doi.org/10.1007/s42773-024-00408-0
Schmidt, H.-P., Abiven, S., Cowie, A., Glaser, B., Joseph, S., Kammann, C., Lehmann, J., Leifeld, J., Pan, G., Rasse, D., Rumpel, C., Woolf, D., Zimmerman, A.R., Hagemann, N., 2025. Biochar Permanence—A Policy Commentary. GCB Bioenergy 17, e70092. https://doi.org/10.1111/gcbb.70092
Schmidt, H.-P., Abiven, S., Hagemann, N., 2022. Permanence of soil applied biochar. An executive summary for Global Biochar Carbon Sink certification. The Biochar Journal 69–74.
Schmidt, H.-P., Anca-Couce, A., Hagemann, N., Werner, C., Gerten, D., Lucht, W., Kammann, C., 2019. Pyrogenic carbon capture and storage. GCB Bioenergy 11, 573–591. https://doi.org/10.1111/gcbb.12553
Schmidt, H.-P., Kammann, C., Hagemann, N., 2024. Certification of the carbon sink potential of biochar.
Schmidt, H.-P., Kammann, C., Hagemann, N., Leifeld, J., Bucheli, T.D., Sánchez Monedero, M.A., Cayuela, M.L., 2021. Biochar in agriculture – A systematic review of 26 global meta-analyses. GCB Bioenergy 13, 1708–1730. https://doi.org/10.1111/gcbb.12889
Setia, R., Rengasamy, P., Marschner, P., 2014. Effect of mono- and divalent cations on sorption of water-extractable organic carbon and microbial activity. Biol Fertil Soils 50, 727–734. https://doi.org/10.1007/s00374-013-0888-1
Shukla, P.R., Skea, J., Calvo Buendia, E., Masson-Delmotte, V., Pörtner, H.-O., Roberts, D.C., Zhai, P., Slade, R., Connors, S.L., van Diemen, R., Ferrat, M., Haughey, E., Luz, S., Neogi, S., Pathak, M., Petzold, J., Portugal-Pereira, J., Vyas, P., Huntley, E., Kissick, K., Belkacemi, M., Malley, J. (Eds.), 2022. Climate Change and Land: IPCC Special Report on Climate Change, Desertification, Land Degradation, Sustainable Land Management, Food Security, and Greenhouse Gas Fluxes in Terrestrial Ecosystems, 1st ed. Cambridge University Press. https://doi.org/10.1017/9781009157988
Sinsabaugh, R.L., Manzoni, S., Moorhead, D.L., Richter, A., 2013. Carbon use efficiency of microbial communities: stoichiometry, methodology and modelling. Ecology Letters 16, 930–939. https://doi.org/10.1111/ele.12113
Smith, S.M., Fuss, S., Buck, H., Schenuit, F., Pongratz, J., Schulte, I., Lamb, W.F., Probst, B., Edwards, M., Nemet, G.F., Cox, E., Vaughan, N., Injy Johnstone, Geden, O., Burke, J.,

Gidden, M., Roe, S., Müller-Hansen, F., Minx, J., 2024. The State of Carbon Dioxide Removal - 2nd Edition. OSF.
Sohng, J., Sokol, N.W., Whiteaker, S., Schmidt, R., Holzer, I., Goertzen, H., Peña, J., Houlton, B.Z., Montañez, I., O'Geen, A., Scow, K., 2025. Combining organic amendments with enhanced rock weathering shifts soil carbon storage in croplands. Science of The Total Environment 998, 180179. https://doi.org/10.1016/j.scitotenv.2025.180179
Steinwidder, L., Boito, L., De Schutter, A., Frings, P.J., Miladinović, N., Niron, H., Rijnders, J., Roussard, J., Van Acker, K., Van Gerven, T., Vienne, A., Watjanatepin, P., Vicca, S., 2026. Higher Inorganic CO_2 Removal Despite Slower Weathering in an Enhanced Weathering Experiment With Steel Slags and Basalt. Global Change Biology 32, e70666. https://doi.org/10.1111/gcb.70666
Steinwidder, L., Boito, L., Frings, P.J., Niron, H., Rijnders, J., de Schutter, A., Vienne, A., Vicca, S., 2025. Beyond Inorganic C: Soil Organic C as a Key Pathway for Carbon Sequestration in Enhanced Weathering. Global Change Biology 31, e70340. https://doi.org/10.1111/gcb.70340
Su, C., Kang, R., Huang, W., Wang, A., Li, X., Huang, K., Zhou, Q., Fang, Y., 2025. CO2 removal with enhanced wollastonite weathering in acidic and calcareous soils. Soil Ecol. Lett. 7, 240273. https://doi.org/10.1007/s42832-024-0273-z
Sun, F., Lu, S., 2014. Biochars improve aggregate stability, water retention, and pore-space properties of clayey soil. Journal of Plant Nutrition and Soil Science 177, 26–33. https://doi.org/10.1002/jpln.201200639
Swoboda, P., Döring, T.F., Hamer, M., 2022. Remineralizing soils? The agricultural usage of silicate rock powders: A review. Science of The Total Environment 807, 150976. https://doi.org/10.1016/j.scitotenv.2021.150976
Tan, K.H., 2010. Principles of Soil Chemistry, 0 ed. CRC Press. https://doi.org/10.1201/9781439894606
Te Pas, E.E.E.M., Chang, E., Marklein, A.R., Comans, R.N.J., Hagens, M., 2025. Accounting for retarded weathering products in comparing methods for quantifying carbon dioxide removal in a short-term enhanced weathering study. Front. Clim. 6, 1524998. https://doi.org/10.3389/fclim.2024.1524998
Te Pas, E.E.E.M., Comans, R.N.J., Bisseling, S., Hagens, M., 2026. Enhanced weathering and biochar co-deployment boosts CO2 sequestration through changing soil properties. Geoderma 466, 117668. https://doi.org/10.1016/j.geoderma.2025.117668
Te Pas, E.E.E.M., Hagens, M., Comans, R.N.J., 2023. Assessment of the enhanced weathering potential of different silicate minerals to improve soil quality and sequester CO2. Front. Clim. 4, 954064. https://doi.org/10.3389/fclim.2022.954064
Vicca, S., Goll, D.S., Hagens, M., Hartmann, J., Janssens, I.A., Neubeck, A., Peñuelas, J., Poblador, S., Rijnders, J., Sardans, J., Struyf, E., Swoboda, P., Van Groenigen, J.W., Vienne, A., Verbruggen, E., 2022. Is the climate change mitigation effect of enhanced silicate weathering governed by biological processes? Global Change Biology 28, 711–726. https://doi.org/10.1111/gcb.15993
Vienne, A., Frings, P., Poblador, S., Steinwidder, L., Rijnders, J., Schoelynck, J., Vinduskova, O., Vicca, S., 2024. Earthworms in an enhanced weathering mesocosm experiment: Effects on soil carbon sequestration, base cation exchange and soil CO2 efflux. Soil Biology and Biochemistry 199, 109596. https://doi.org/10.1016/j.soilbio.2024.109596
Vienne, A., Frings, P., Rijnders, J., Boito, L., Hartmann, J., Niron, H., Poetra, R., Estrada, M.P., Reershemius, T., Steinwidder, L., Suhrhoff, T.J., Vicca, S., 2026a. Weathering without

realizing inorganic CO_2 removal revealed through base cation monitoring. SOIL 12, 421–440. https://doi.org/10.5194/soil-12-421-2026

Vienne, A., Newell, J., Roussard, J., Doherty, R., Cox, S.F., Lyons, G., Vicca, S., 2026b. Effects of basalt and biochar addition on base cations and trace metals in plants and soil in an urban field trial. Biogeosciences 23, 1681–1695. https://doi.org/10.5194/bg-23-1681-2026

Vienne, A., Poblador, S., Portillo-Estrada, M., Hartmann, J., Ijiehon, S., Wade, P., Vicca, S., 2022. Enhanced Weathering Using Basalt Rock Powder: Carbon Sequestration, Co-benefits and Risks in a Mesocosm Study With Solanum tuberosum. Front. Clim. 4, 869456. https://doi.org/10.3389/fclim.2022.869456

Vorrath, M.-E., Amann, T., Meyer zu Drewer, J., Hagemann, N., Aldrich, C., Börker, J., Seedtke, M., Becker, J.N., Hagens, M., Eschenbach, M., Hartmann, J., 2025. Pyrogenic carbon and Carbonating Minerals for Carbon Capture and Storage (PyMiCCS) Part II: Organic and Inorganic Carbon Dioxide Removal in an Oxisol. Frontiers in Climate. https://doi.org/10.3389/fclim.2025.1592454

Vorrath, M.-E., Amann, T., Meyer zu Drewer, J., Linke, T., Feiertag, L., Nauenburg, S., Maslouski, M., Ansari, M., Eschenbach, A., Hagemann, N., Hartmann, J., in prep. Soil-Dependent Controls of Carbon Dioxide Removal from combined Enhanced Rock Weathering and Biochar in different Soils. Applied Geochemistry.

Vorrath, M.-E., Haque, F., Stoeck, L., Aldrich, C., Kiddell, M., Smet, I., in prep. Hot, hotter, thermal activation: how to boost weathering rates of serpentine-rich rocks for carbon dioxide removal. Geoscience Data Journal.

Wang, J., Xiong, Z., Kuzyakov, Y., 2016. Biochar stability in soil: meta-analysis of decomposition and priming effects. GCB Bioenergy 8, 512–523. https://doi.org/10.1111/gcbb.12266

Wang, Y., Wang, H.-S., Tang, C.-S., Gu, K., Shi, B., 2022. Remediation of heavy-metal-contaminated soils by biochar: a review. Environmental Geotechnics 9, 135–148. https://doi.org/10.1680/jenge.18.00091

Wang, Y., Xiao, X., Chen, B., 2018. Biochar Impacts on Soil Silicon Dissolution Kinetics and their Interaction Mechanisms. Sci Rep 8, 8040. https://doi.org/10.1038/s41598-018-26396-3

Wang, Z.-L., Li, Y.-F., Jiang, P.-K., Zhou, G.-M., Liu, J., 2014. Effect of bamboo leaf biochar addition on soil CO2 efflux and labile organic carbon pool in a Chinese chestnut plantation. Ying Yong Sheng Tai Xue Bao 25, 3152–3160.

Waring, B.G., Gurgel, A., Köberle, A.C., Paltsev, S., Rogelj, J., 2023. Natural Climate Solutions must embrace multiple perspectives to ensure synergy with sustainable development. Front. Clim. 5, 1216175. https://doi.org/10.3389/fclim.2023.1216175

West, T.O., McBride, A.C., 2005. The contribution of agricultural lime to carbon dioxide emissions in the United States: dissolution, transport, and net emissions. Agriculture, Ecosystems & Environment 108, 145–154. https://doi.org/10.1016/j.agee.2005.01.002

Wilson, M.J., 1999. The origin and formation of clay minerals in soils: past, present and future perspectives. Clay Minerals 34, 7–25. https://doi.org/10.1180/000985599545957

Xu, T., Yuan, Z., Vicca, S., Goll, D.S., Li, G., Lin, L., Chen, H., Bi, B., Chen, Q., Li, C., Wang, X., Wang, C., Hao, Z., Fang, Y., Beerling, D.J., 2024. Enhanced silicate weathering accelerates forest carbon sequestration by stimulating the soil mineral carbon pump. Global Change Biology 30, e17464. https://doi.org/10.1111/gcb.17464

Yang, F., Xu, Z., Huang, Y., Tsang, D.C.W., Ok, Y.S., Zhao, L., Qiu, H., Xu, X., Cao, X., 2021. Stabilization of dissolvable biochar by soil minerals: Release reduction and organo-

mineral complexes formation. Journal of Hazardous Materials 412, 125213. https://doi.org/10.1016/j.jhazmat.2021.125213

Yu, Y., Liu, D., Wu, H., 2014. Formation and Characteristics of Reaction Intermediates from the Fast Pyrolysis of NaCl- and MgCl2-Loaded Celluloses. Energy Fuels 28, 245–253. https://doi.org/10.1021/ef401483u

Zhu, C., Huang, K., Xue, M., Zhang, Y., Wang, J., Liu, L., 2023. Effect of MgCl2 Loading on the Yield and Performance of Cabbage-Based Biochar. Bioengineering (Basel) 10, 836. https://doi.org/10.3390/bioengineering10070836

Supplementary Information

Table of content

S1. Grain size distribution

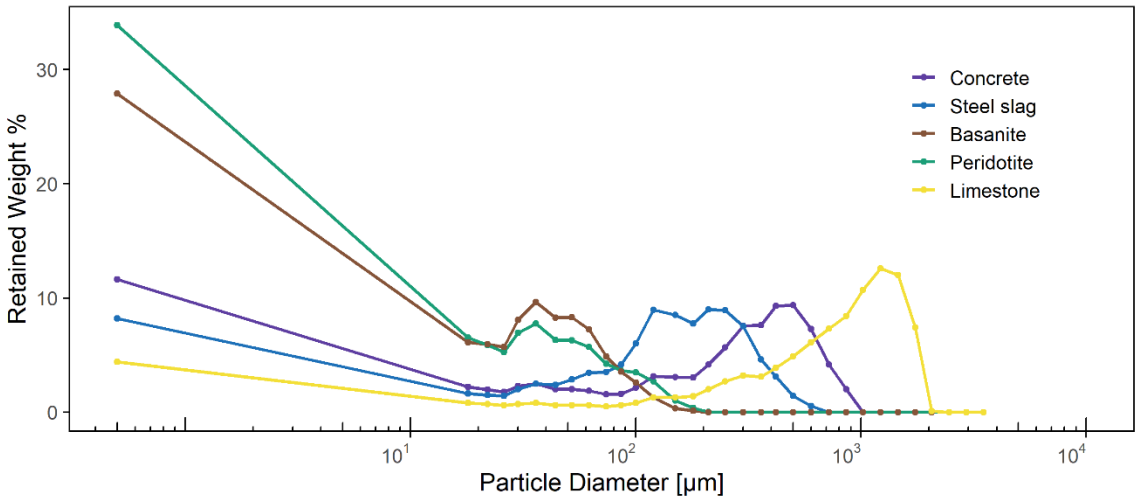

Figure S1. Grain size distribution of mineral feedstock samples concrete, steel slag, basanite, peridotite and limestone.

S2. Pyrolysis of biochar and RE-biochars and hydropyrolysis

Pyrolysis

All biochar and RE-biochars were pyrolyzed in a PYREKA pyrolysis unit from *Novocarbo* in Dörth, Germany. The PYREKA unit consists of a continuous auger reactor with a diameter of 8cm. The reactor is purged with N2 at flowrates of 2.5 L min^{-1}. To achieve the highest heating temperature of the pyrolysis process, the reactor is heated to 650°C. All thermal conversions were carried out at this temperature, with a residence time of approx. 15 minutes. To ensure that there is no intrusion of oxygen or disruptions in the reactor temperature, the feedstock inlet is separated from the reactor by a rotary valve. After the pyrolysis process, the resulting materials are cooled down to ambient temperatures while being protected from oxygen exposure. This is achieved by utilizing the N2 purged outlet of the PYREKA unit.

Hydropyrolysis

Hydropyrolysis (HyPy) was conducted as outlined by Meredith et al. (2017). In summary, milled samples were combined with 10 wt% ammonium molybdate-tetrahydrate as a catalyst. The samples were heated in a reactor under 150 bar of hydrogen pressure, starting from ambient temperature to 250 °C at a rate of 300 °C min^{-1}. They were then raised from 250 °C to 550 °C at 8 °C min^{-1} and maintained at that temperature for 2 minutes. The residues after HyPy were weighed and analysed for C_{org}. This residue is categorized as stable polycyclic aromatic carbon, containing more than 7 fused aromatic rings that exhibit high environmental stability (Schmidt et al., 2022). This mass remaining of the initial C_{org} content is expressed as BC_{HyPy}.

S3. Characteristics of the sand soil

Table S1. Key properties and grain-size distribution of the sandy soil. All data and methodological details are reported in Ansari et al. (2026).

Physico-chemical properties		
pH in H_2O		5.6
pH in $CaCl_2$		4.7
Electric conductivity	µS cm^{-1}	47.7
Total carbon	wt%	1.24
Total inorganic carbon	wt%	0.04
Organic carbon	wt%	1.2
Total nitrogen	wt%	0.1
OC/N_{tot}		11.3
Cation exchange capacity	mmolc kg^{-1}	21
Base saturation	%	140.7
Water capacity	%	0.6
Water holding capacity	%	35.5

Grain size distribution in wt%	
Coarse sand	2.3
Middle sand	50
Coarse fine sand	33.3
Fine fine sand	8.1
Coarse silt	1.2
Middle silt	0.8
Fine silt	0.5
Clay	3.7

S4. Experimental setup

To initiate the incubation process, acrylic tubes were used as soil columns (25 mm length, 56 mm inner diameter) that were sealed at the bottom with a 5 µm plankton net. For each batch, duplicates of 500 g of sand were mixed with a specific material, filled into the columns, and lightly tapped to allow the soil to settle. For single and co-applications either 10g of biochar and/or 9.9g of mineral were used, for RE-biochars the mass of material was adjusted to contain 9.9g of mineral which resulted in 15 to 16.3g. The single materials, the co-deployment of biochar and minerals as well as RE-biochars and several control columns made up 38 columns in total. The columns were placed vertically in two gas-sealed incubators which were regularly flushed with a N_2+CO_2 gas mixture to maintain an atmosphere of pCO_2 of 1.5%. Due to diffusion of gas a CO_2 level of 1.0% ± 0.4 (box 1) and 1.2% ± 0.6 (box 2) was maintained over the experiment period (Figure S2). Prior to the experiment, the columns were saturated by soaking them with 250 ml of deionised water (DI). During the experiment, the columns were rinsed with DI, which had been gasified with the corresponding N_2+CO_2 gas mixture until equilibration. This process aimed to simulate rainwater in equilibrium with the pCO_2 of the soil environment within the incubator. According to PhreeqC, the target values were a pH of 4.806 and an EC of 5 µS cm^{-1} at 20 °C. To mimic an annual rainfall of 820 mm, the columns were rinsed three times a week with 12.9 ml of DI. The leachate water resulting from this rinsing process was collected in 250 ml polyethylene bottles positioned beneath the columns. The experiments were carried out over a period of 75 weeks in a dark room, maintaining an approximate temperature of 22.3°C ± 1.8. Sampling intervals were progressively extended over time, starting at two-week intervals and increasing to twelve-week intervals. The specific sampling weeks were as follows: week 2, 4, 6, 9, 15, 19, 27, 39, 51, 63 and 75. The first box was also sampled in week 87 but this data was only for chemical flux monitoring (Figure S6-9 in S11-12) and not used for any calculations in this study.

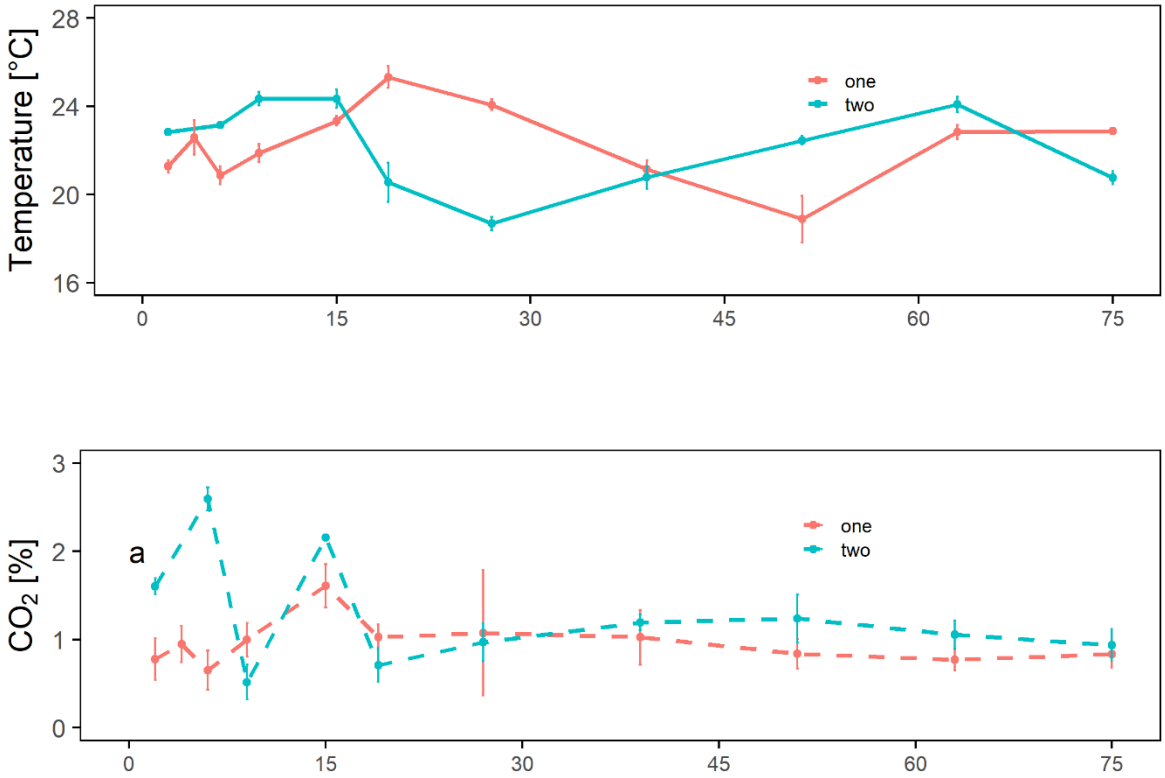

Figure S2. Temperature and CO_2 levels in the incubator boxes during the experiment. Error bars indicate standard deviations, n=18.

S5. Leachate analyses

The sampling and analyses of the leachates during the incubation experiment were done according to Vorrath et al. (2025). At each sampling time, dissolved inorganic carbon (DIC) was sampled directly inside the incubator to prevent re-equilibration with the lab atmosphere. Trace metals were as well sampled directly inside the incubator, acidified (1 ml of 14 M HNO_3) and pooled after experiment weeks 9 and 27. Outside the incubator, pH, temperature, and EC of the leachate were immediately measured with a WTW 3630 IDS Multimeter. For total alkalinity (TA), major ion chromatography, and dissolved silica (DSi), samples were passed through a 0.45 µm PES syringe filter and analysed within 48 hours to reduce changes caused by precipitation of minerals that may be supersaturated. Samples for dissolved organic carbon (DOC) were filtered using pre-combusted glass fibre filters with an approximate pore size of 0.45 µm (Whatman GF/F). All samples were kept cool and protected from light until analysis. Additionally, pH, EC, TA, and major ions were also determined for the mineral suspension in the same way.

The analyses of DIC, TA, DSi, DOC and major ions was described in Vorrath et al. (2025). DIC samples were analysed using a Picarro G2131-I cavity ring-down spectrometer coupled with an AutoMate FX preparation device. Total alkalinity was determined via automated titration to pH 4.3 using a Metrohm Titrando titrator with 0.02 N HCl, following the procedure described by Dickson (1981). Calibration was performed against two in-house standards, with an error margin below 1%. Major cations (Na^+, K^+, Ca^{2+}, Mg^{2+}) and anions (Cl^-, SO_4^{2-}) were analysed through ion chromatography using a Metrohm 881 Compact IC Pro system, achieving an error rate of less than 5%. Dissolved silica was measured using the molybdate blue colorimetric method as described by Hansen and Koroleff (1999). The average coefficient of variation for all measurements was 0.6 ± 0.8%. DOC concentrations were determined with a Shimadzu TOC-VCSH Analyzer, utilizing high-temperature combustion and non-dispersive infrared detection. The trace metals copper (Cu), chromium (Cr), cadmium (Cd), lead (Pb), and nickel (Ni) were determined via atomic absorption spectroscopy (AAS). The instrument was calibrated using appropriate standard solutions by measuring absorbance at specific wavelengths (Cu at 324.7 nm, Cr at 357.9 nm, Cd at 228.8 nm, Pb at 283.3 nm, and Ni at 232.0 nm) and metal concentration

of each sample was quantified by comparison to these standards. Acceptable errors were within 0.5%.

S6. Calculations of chemical fluxes, alkalinity production rates, different carbon sinks and the soil carbon and cation budgets

Chemical fluxes

The fluxes of element x (Fx) per interval I is calculated following Amann et al. (2022)

$$F_{x,i} = \left(c_{x,i} * Q_{rain,i}\right) / \, t_i \qquad \text{Eq. 1}$$

Where c_x represents the element concentration (mol L^{-1}), Q_{rain} (L) is the volume of irrigation per interval, and t_i is the number of weeks per interval (days). To calculate the total elements released over the experiment duration of 75 weeks they are summed as:

$$F_{tot,i} = \sum_{t=1}^{75} F_{x,i} \qquad \text{Eq. 2}$$

Alkalinity production rates

For all inorganic carbon fluxes, the carbonate alkalinity (CA) was derived from measured values of DIC, pH, temperature, and cation concentrations using PhreeqC (Parkhurst and Appelo, 2013) (database: phreeqc.dat) to exclude contributions from organic alkalinity (Rieder et al., 2026). The weekly net production rate of carbonate alkalinity (CA_{prod}) per unit mass of soil amendment was calculated using the amount of CA released, according to the following equation:

$$CA_{prod} = Q_{rain}(t_i) \times c_{TA}(t_i) * \frac{mass_{amendment}}{100} \div t_i \qquad \text{Eq. 3}$$

where Q_{rain} (L) represents the irrigation volume per column during sampling interval t_i, c_{CA} (mol L^{-1}) is the CA at time t_i, $mass_{amendment}$ (g) refers to the mass of the respective soil amendment, and t_i denotes the number of weeks since the previous sampling event. The net CA_{prod} was used to extrapolate mineral weathering of rock amendments and determine after how many weeks the values reached 0 and how much CA had been released in this time. For this, only CA_{prod} values of weeks 39-75 were used to generate a linear model for each amendment (a + b*week, Table S2) as in this time a stable alkalinity flux was observed. This model was then used to estimate the duration during which CA_{prod} indicated positive net fluxes.

Table S2: Coefficients a and b derived from the linear model for each mineral amendment to be used for a linear extrapolation of CA_{prod} = a*week + b.

	a	b
Concrete	-0.001	8.966
Steel slag	-0.076	12.169
Basanite	-0.005	2.630
Peridotite	-0.012	2.897
Limestone	-0.021	8.015

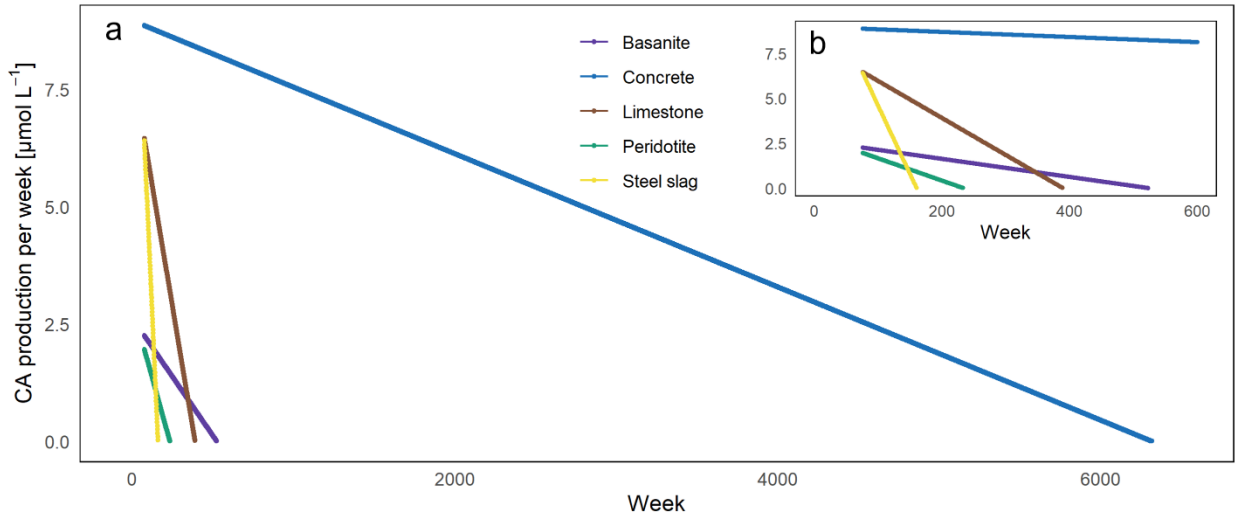

Figure S3: Extrapolation of the carbonate alkalinity production (CA_{prod}) of mineral feedstocks. a) The extrapolation starts in week 76 and runs until CA_{prod} reaches 0 for each individual material. The extrapolation of concrete had to be stopped in week 2022 when the full IC-$Sink_{pot}$ was realised. b) Detailed view on the first 600 weeks of extrapolation.

Calculations of potential carbon sinks

The potential carbon sink from inorganic carbon based on alkalinity release from mineral weathering, the IC-Sink (IC-$Sink_{pot}$, $kgCO_2\ t^{-1}$), was calculated by:

$$IC - Sink_{pot}\ of\ Rock = \frac{Rock_{fraction}}{100} * CDR_{rock\ powder} \quad \text{Eq. 4}$$

where the rock fraction of the amended material is $Rock_{fraction}$ (%), and $CDR_{rock\ powder}$ ($kgCO_2\ t^{-1}$) is the CDR potential of the according rock powder calculated after Renforth (2019) (values see supplementary data D2). Neither for the CDR potential nor for the IC-sinks wasthe potential downstream CO_2 loss due to surface water re-equilibration as proposed by Renforth (2019) applied to keep CO_2 values comparable to values from DOC in this study and comparable to other studies in general. Since the experiments were performed in darkness without plants or fauna, nutrient uptake was not considered (Dietzen and Rosing, 2023).

The IC-$Sink_{pot}$ from inorganic carbon based on alkalinity release from biochar is calculated as

$$IC - Sink_{pot}\ of\ Biochar = \frac{Biochar_{fraction} * PIC_{biochar}}{100} / M_C * M_{CO_2} \qquad \text{Eq. 5}$$

where the fraction of biochar is $Biochar_{fraction}$ (%) and the particulate inorganic carbon (PIC) in biochar is $PIC_{biochar}$ (%). The molar masses are defined as 44.01 g mol^{-1} for CO_2 (M_{CO2}) and 12.01 g mol^{-1}, for carbon (M_C).

The IC-$Sink_{pot}$ from inorganic carbon based on alkalinity release from biochar carbonates in RE-biochars is calculated as

$$IC - Sink_{pot}\ of\ RE - Biochar = \frac{Biochar_{fraction}}{100} * \frac{\left(\frac{Biochar_{fraction} * PIC_{biochar}}{100}\right) - \left(\frac{Rock_{fraction} * PIC_{rock}}{100}\right)}{\frac{Biochar_{fraction} * 100}{100}} / M_C * M_{CO_2} \qquad \text{Eq. 5}$$

by utilizing the fractions of rock in RE-biochars ($Rock_{fraction}$, %) and the particulate inorganic carbon (PIC) of the rock (PIC_{rock}, %), and with the RE-biochar fraction ($RE\text{-}biochar_{fraction}$, %), the PIC in RE-biochar ($PIC_{RE\text{-}biochar}$, %), and the fraction of biochar ($Biochar_{fraction}$, %) in RE-biochar. The molar mass of CO_2 M_{CO2} is 44.01 g mol^{-1} and of carbon M_C is 12.01 g mol^{-1}.

The carbon sink from pyrogenic carbon in biochar, the PyC-Sink, at the day of application was calculated with:

$$PyC - Sink = \frac{C_{org_{(RE-)biochar}}}{100} * \frac{100 - (RE-)biochar_{ashfraction}}{100} / M_C * M_{CO_2} \quad \text{Eq. 7}$$

with the C_{org} of all (RE-)biochars ($C_{org(RE-)biochar}$, %), the ash fraction of (RE-)biochars ($(RE-)biochar_{ashfraction}$, %), and the molar mass of CO_2 M_{CO2} (44.01 g mol^{-1}) and carbon M_C (12.01 g mol^{-1}). For an estimation of long-term carbon storage, the PyC-Sink$_{long}$ was multiplied with the amount of BC_{HyPy} from the HyPy analysis. To avoid overestimation, the C_{org} decay considered to happen over 1000 years was also applied on the experiment duration of 75 weeks as most of the PyC-Sink loss occurs within the first year of soil application.

For the total C-Sink$_{pot}$, the IC-Sink$_{pot}$ of rock, biochar or RE-biochar and the PyC-Sink$_{pot}$ are summed according to their fraction in the amendment.

To calculate the equivalent of CO_2 from concentration of DOC (c_{DOC}) in the leachate water, the measured DOC is multiplied with 44.01 g mol^{-1} for CO_2 (M_{CO2}).

$$CO_2\ from\ DOC = c_{DOC} * M_{CO_2} \quad \text{Eq. 8}$$

Calculation of deviations of measured from expected C-Sinks

To identify synergistic effects, the deviation of the measured from the expected C-Sinks (carbon sinks from both inorganic and pyrogenic carbon) of co-application and (RE-)biochar amendments is estimated based on individual biochar and mineral amendment. The expected C-Sink (C-Sink$_{expected}$) is determined as:

$$C - Sink_{expected} \quad \text{Eq. 9}$$
$$= (IC - sink_{pure\ biochar} * biochar\ content)$$
$$+ (IC - sink_{pure\ rock} * rock\ content)$$
$$+ (PyC - sink * biochar\ content)$$

where, for every specific soil amendment, the IC-Sink of the single biochar amendment ($IC\text{-}Sink_{pure\ biochar}$) is multiplied with the biochar content, the IC-Sink of the single rock amendment ($IC\text{-}Sink_{pure\ rock}$) is multiplied with the rock content and the PyC-Sink is multiplied with the biochar

content. To calculate the expected IC-Sink (*IC-Sink*$_{expected}$) the PyC-Sink is not considered in the equation.

The deviation of the measured C-Sink from the expected C-Sink is calculated as:

$$Deviation\ measured\ C-Sink\ \% = \frac{C-Sink_{measured}-C-Sink_{expected}}{C-Sink_{expected}} * 100 \quad \text{Eq. 10}$$

where, for every specific soil amendment, the *C-Sink*$_{measured}$ is the measured value and the *C-Sink*$_{expected}$ is determined after equation 9.

The deviation of the measured IC-Sink and expected IC-Sink is calculated as:

$$Deviation\ measured\ IC-Sink\ \% \quad \text{Eq. 11}$$
$$= \frac{IC-Sink_{measured} - (IC-Sink_{expected\ rock} - IC-Sink_{expected\ biochar})}{IC-Sink_{expected\ rock} + IC-Sink_{expected\ biochar}} * 100$$

where the *IC-Sink*$_{measured}$ is the measured CA in the leachate and the *IC-Sink*$_{expected\ rock}$ and *IC-Sink*$_{expected\ biochar}$ are the expected IC-Sinks of each rock and biochar.

To determine the deviation from the measured geogenic IC-Sink from the expected geogenic IC-Sink, the IC-Sink from biochar is treated as a constant and the remaining IC-Sink is attributed to mineral weathering:

$$Deviation\ measured\ geogenic\ IC-sink\ \% \quad \text{Eq. 12}$$
$$= \frac{IC-Sink_{measured} - IC-Sink_{expected\ biochar} - IC-Sink_{expected\ rock}}{IC-Sink_{expected\ rock}} * 100$$

Calculation of soil carbon budget

To assess changes in organic and inorganic soil carbon pools, the initial carbon pool (initial C_{pool}) of each soil column was compared to the post-experiment soil column. This comparison considers:

$$Initial\ C_{pool} = IC_{soil} + C_{org\ soil} + IC_{rock} + C_{org\ rock} + IC_{(RE-)biochar} + C_{org\ (RE-)biochar} \quad \text{Eq. 13}$$

using the inorganic soil carbon (IC_{soil}), the organic soil carbon ($C_{org\ soil}$), the inorganic carbon from the rock (IC_{rock}), the organic carbon of rock powder ($C_{org\ rock}$), the inorganic carbon from (RE-)biochars ($IC_{(RE-)biochar}$) and the organic carbon of (RE-)biochars ($C_{org(RE-)biochar}$).

The final C_{pool} after the experiment was determined as

$$Final\ C_{pool} = IC_{soil} + C_{org\ soil} + IC_{leachate} + C_{org\ leachate} \quad \text{Eq. 14}$$

with the inorganic soil carbon (IC_{soil}), the organic soil carbon ($C_{org\ soil}$) the sum of inorganic carbon from all DIC leachate measurements ($IC_{leachate}$) and the sum of C_{org} from all DOC leachate measurements ($C_{org\ leachate}$).

Calculation of major cation budget

The change of the major cation budget throughout the experiment was determined by comparison of the initial $Cation_{pool}$ to the final $Cation_{pool}$:

$$Initial\ Cation_{pool} = Cation_{rock} + Cation_{(RE-)biochar} + Cation_{soilCECcontrol} \quad \text{Eq. 15}$$

with cations added from rock powder ($Cation_{rock}$), and cations added from biochar ($Cation_{(RE-)biochar}$) and $Cation_{soilCECcontrol}$ representing the cations in the control soil leached during the analysis of cation exchange capacity after the experiment. The final $Cation_{pool}$ is based on

$$Final\ Cation_{pool} = Cation_{soilCEC} + Cation_{leachate} \quad \text{Eq. 16}$$

where $Cation_{soilCEC}$ represents cations leached from exchangeable sites of individual amendments, and $Cation_{leachate}$ is the sum of the specific cation concentrations from all leachate measurements. The difference between the initial and final cation pools is assumed to represent cations retained in a solid phase, either as part of rock, biochar, in secondary mineral formations, (hydr-)oxides or associated with organic matter.

Calculation of deviations from expected trace metal fluxes

The deviation of the expected trace metal fluxes and measured trace metal fluxes is calculated as:

$$Deviation\ expected\ TM\ flux\ \% = \frac{(TMflux_{pure\ rock} * rockcontent + TMflux_{pure\ biochar} * biocharcontent) - TMflux_{measured}}{TMflux_{pure\ rock} * rockcontent + TMflux_{pure\ biochar} * biocharcontent} * 100 \quad \text{Eq. 17}$$

where the trace metal fluxes of pure rock ($TMflux_{pure\ rock}$) and pure biochar ($TMflux_{pure\ biochar}$) are multiplied with their content in the specific amendments, subtracted from the measured trace metal flux ($TMflux_{measured}$) and divided by the same.

S7. Trace metal fluxes

The concentrations of trace metals show a sharp decline between week 9 and week 27 (indicated with I and II in Figure S4, data in supplementary data D8). Cadmium concentrations were highest for RE-biochar containing steel slag and peridotite as well as single biochar (max. 63.5 nmol L-1). Chromium release was highest in all RE-biochar and co-deployments of basanite and peridotite (maximum 389 nmol L^{-1}), and also both in pure and co-deployment of basanite, peridotite and biochar. Elevated copper and lead concentrations were observed in RE-biochar with steel slag and single biochar reaching up to 3.6 µmol L^{-1} for copper and 2.7 µmol L^{-1} for lead. Nickel release was primarily associated with amendments containing peridotite (maximum 5.0 µmol L^{-1}) and steel slag. When compared with the limits of the German Drinking Water Ordinance, trace metal release from several RE-biochars with steel slag and peridotite exceeds the thresholds for cadmium, nickel, and lead (red line in Figure S4). Further, single biochar amendments, concrete RE-biochar and basanite RE-biochar and co-deployments exceed thresholds for several metals. Notably, nickel and lead thresholds were also exceeded in the control soil during the first sampling interval.

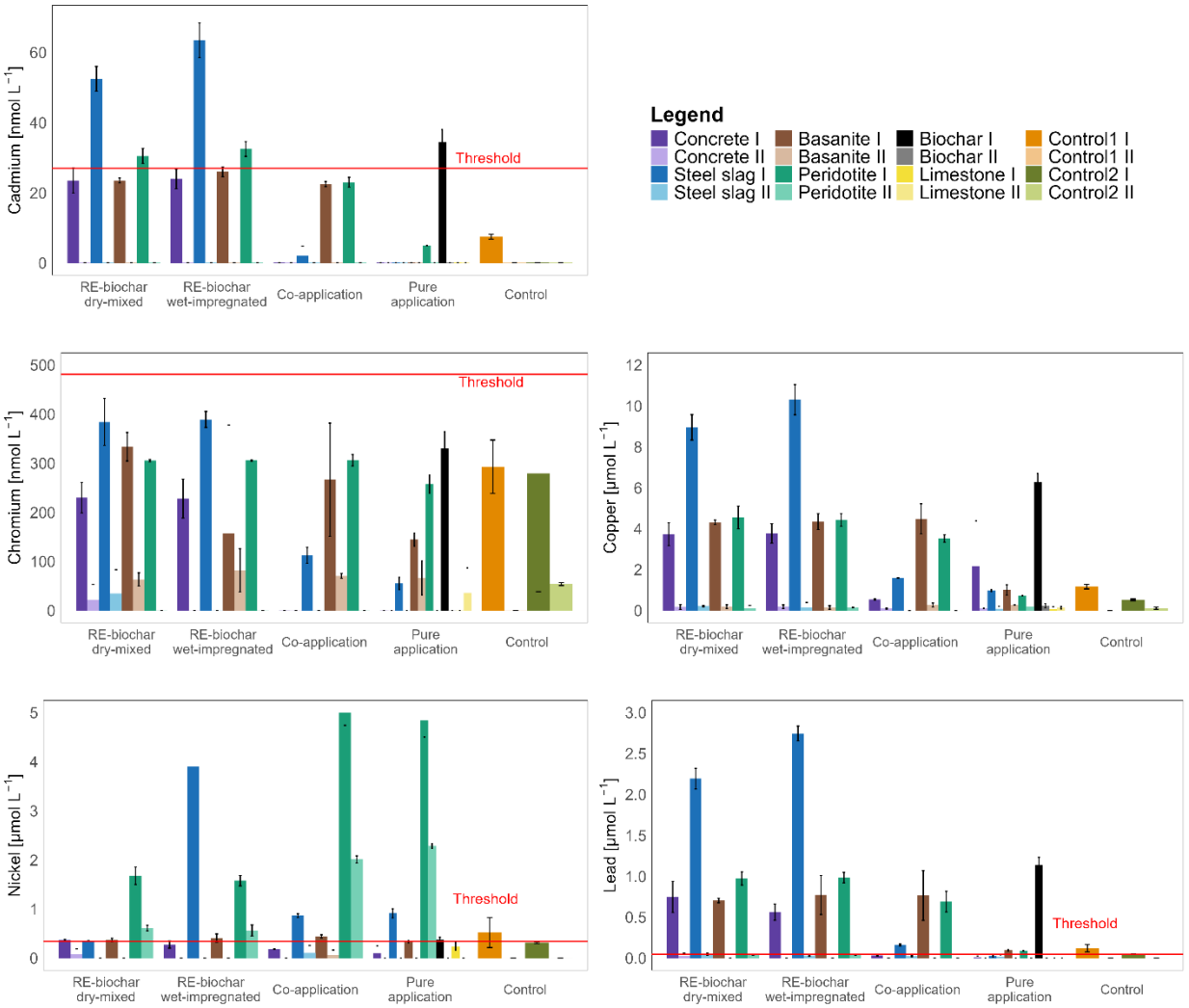

240

241 Figure S4: Concentrations of trace metals from pooled samples after 9 and 27 weeks indicated with I and
242 II, respectively. The thresholds from the German Drinking Water Ordinance are indicated by the red line
243 and are 27 nmol L^{-1} for cadmium, 481 nmol L^{-1} for chromium, 31.3 µmol L^{-1} for copper (not shown in the
244 plot), 0.341 µmol L^{-1} for nickel, and 0.048 µmol L^{-1} for lead. Error bars indicate standard deviations (n=2).
245 Experiments with materials including steel slag, peridotite and biochar were done in box 1 (control 1),
246 while materials including concrete, basanite and limestone were done in box 2 (control 2).

247

S8. Cation budget in the soil

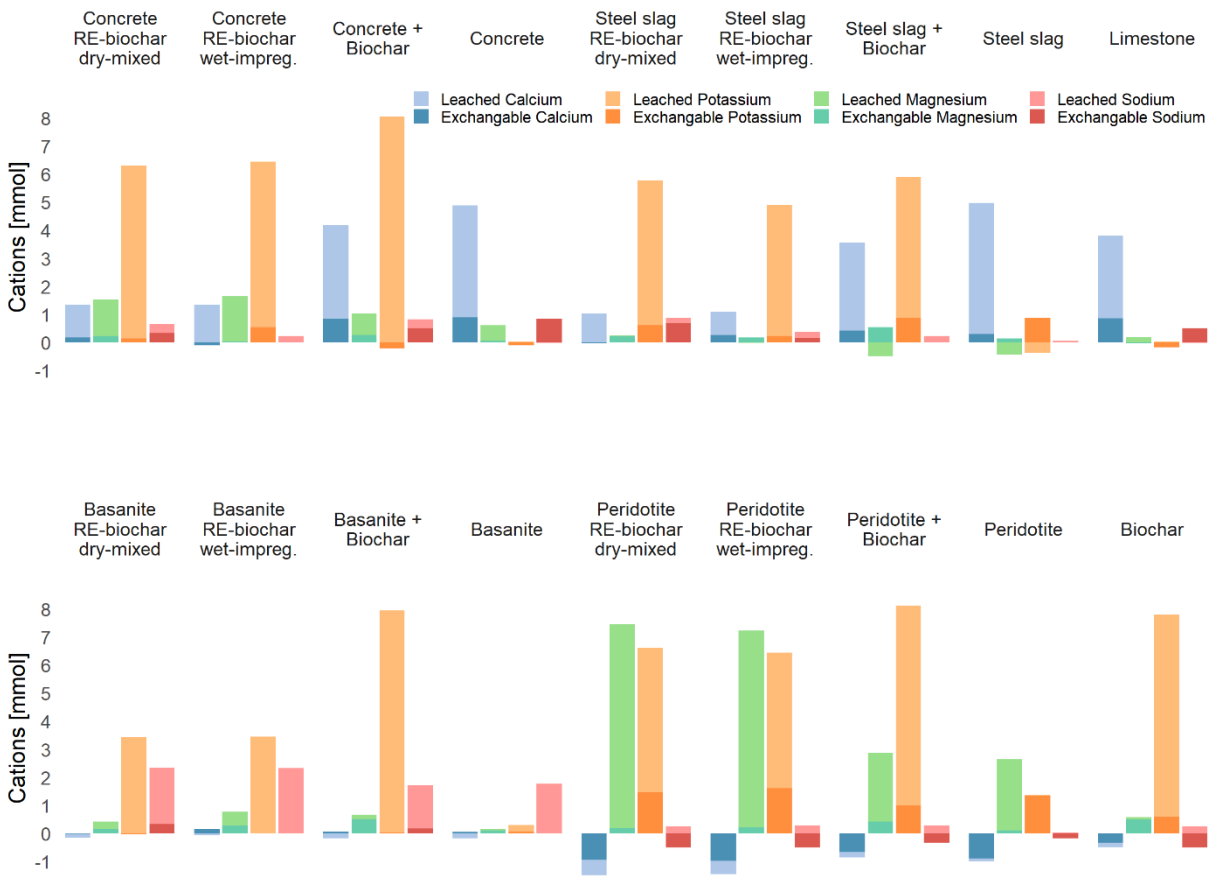

Figure S5: Absolute net values (control values were subtracted from soil amendments) of released major cations measured in the leachate water and exchangeable fraction at the end of the experiment. Negative values for leached cations indicate a retention in the soil, while negative values for the cation in the exchangeable fraction indicates a loss from the soil due to mineral dissolution. Calculations see S6, equations 15 and 16.

256

S9. Description of qualitative assessment of soil amendments

We applied a unified qualitative-scoring approach to compare all amendment configurations based on four key parameters: the experimental C-Sink, the geogenic IC-Sink, DOC leaching, and the additional preparation steps required for each material. To ensure consistency and comparability across these parameters, all measured values were converted into discrete scores ranging from –2 to +2, using percentile thresholds calculated across all configurations where the parameter was measurable (Table S3):

Table S3. Threshold for scoring of parameters.

Thresholds	Score	Experimental C-Sink	Geogenic IC-Sink	DOC leaching	Additional preparation steps
< 10th percentile	-2	< 0.021	< -50.83%	< 14.07	wet-impregnation and pelletizing
10th to 25th percentile	-1	0.021 to 0.199	-50.83 to -23.17%	14.07 to 3.28	dry-mixing and pelletizing
25th to 75th percentile	0	0.199 to 0.979	-23.17 to 23.17%	3.28 to -3.28	-
75th to 90th percentile	1	0.979 to 1.023	23.17 to 50.83%	-3.28 to -14.07	mixing
> 90th percentile	2	> 1.023	> 50.83%	> -14.07	no preparation

For the DOC leaching negative values (indicating DOC retention) were rated positive. We did not consider trace metal content and release as in one of the control soil columns thresholds for nickel and lead were exceeded by these columns. Some materials cannot express certain parameters (e.g., no PyC-Sink in single mineral amendments). These cases were assigned a neutral score of 0. The parameter “additional preparation steps” was evaluated qualitatively, with fewer preparatory requirements receiving higher scores and more complex treatments receiving lower scores. Cases in which a parameter could not be expressed for a given material configuration were assigned a neutral score of 0 and excluded from percentile calculations. The outcome of this assessment is displayed in Table S4.

Table S4: Overview on the scoring of the main parameters that determined the rating of mineral and biochar combinations.

	Experimental C-Sink	Geogenic IC-Sink	DOC leaching	Additional preparation steps	Score	Recommendation
ConcreteChar-dry	0	-1	0	-1	-0.50	Co-application Single application
ConcreteChar-wet	0	-1	0	-2	-0.75	
Concrete + Biochar	2	0	1	1	1.00	
Concrete	-1		2	2	1.00	
SteelslagChar-dry	0	-1	-1	-1	-0.75	Co-application Single application
SteelslagChar-wet	0	-2	-1	-2	-1.25	
Steel slag + Biochar	1	-1	-2	1	-0.25	
Steel slag	-1		-2	2	-0.33	
BasaniteChar-dry	0	0	0	-1	-0.25	Co-application Single application
BasaniteChar-wet	0	0	-1	-2	-0.75	
Basanite + Biochar	1	1	0	1	0.75	
Basanite	-2		0	2	0.00	
PeridotiteChar-dry	0	2	-2	-1	-0.25	Co-application Single application
PeridotiteChar-wet	0	2	-2	-2	-0.50	
Peridotite + Biochar	1	1	-1	1	0.50	
Peridotite	-2		-1	2	-0.33	
Biochar	2		-1	2	1.00	
Limestone	-1		1	2	0.67	

S10. Time series of net DOC fluxes, bulk chemistry, cations and anions

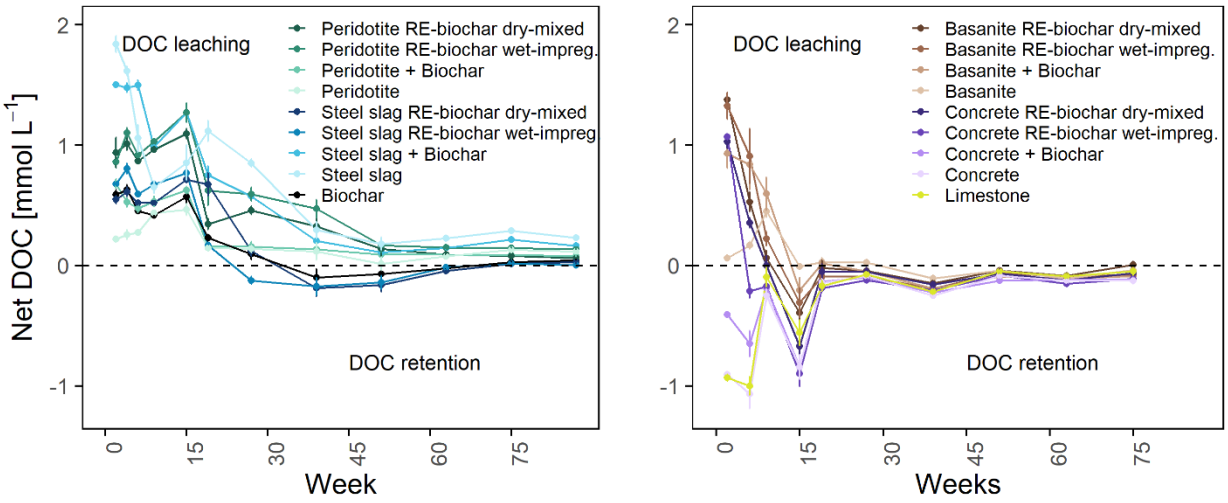

Figure S6. Time series of net DOC fluxes in the leachate water. Error bars indicate standard deviations (n=2).

S11. Time series of leachate analyses

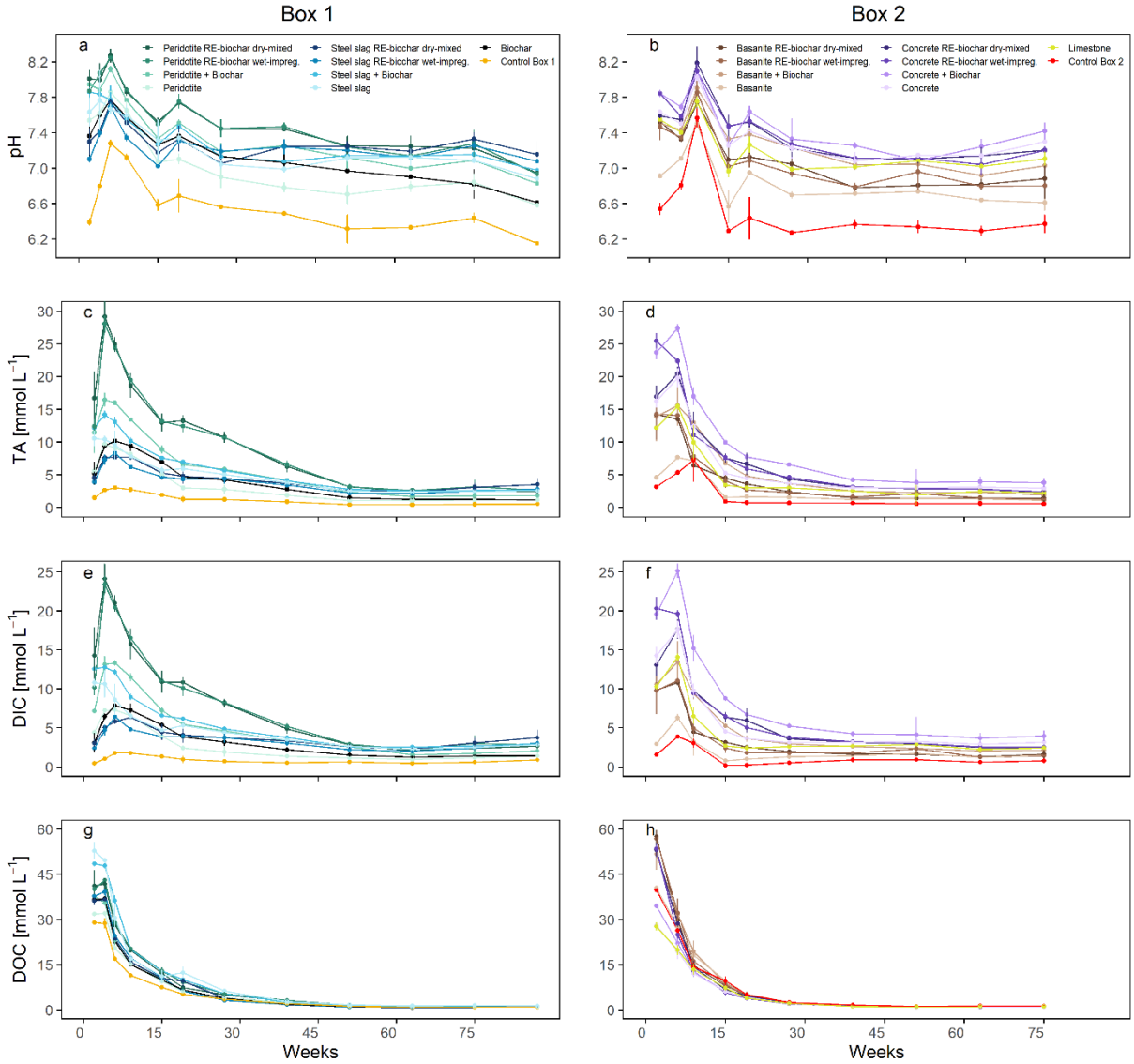

Figure S7. Time series of the bulk chemistry during the experiment with a-b) pH values, c-d) total alkalinity (TA), e-f) dissolved inorganic carbon (DIC), and dissolved organic carbon (DOC). Error bars indicate standard deviations (n=2).

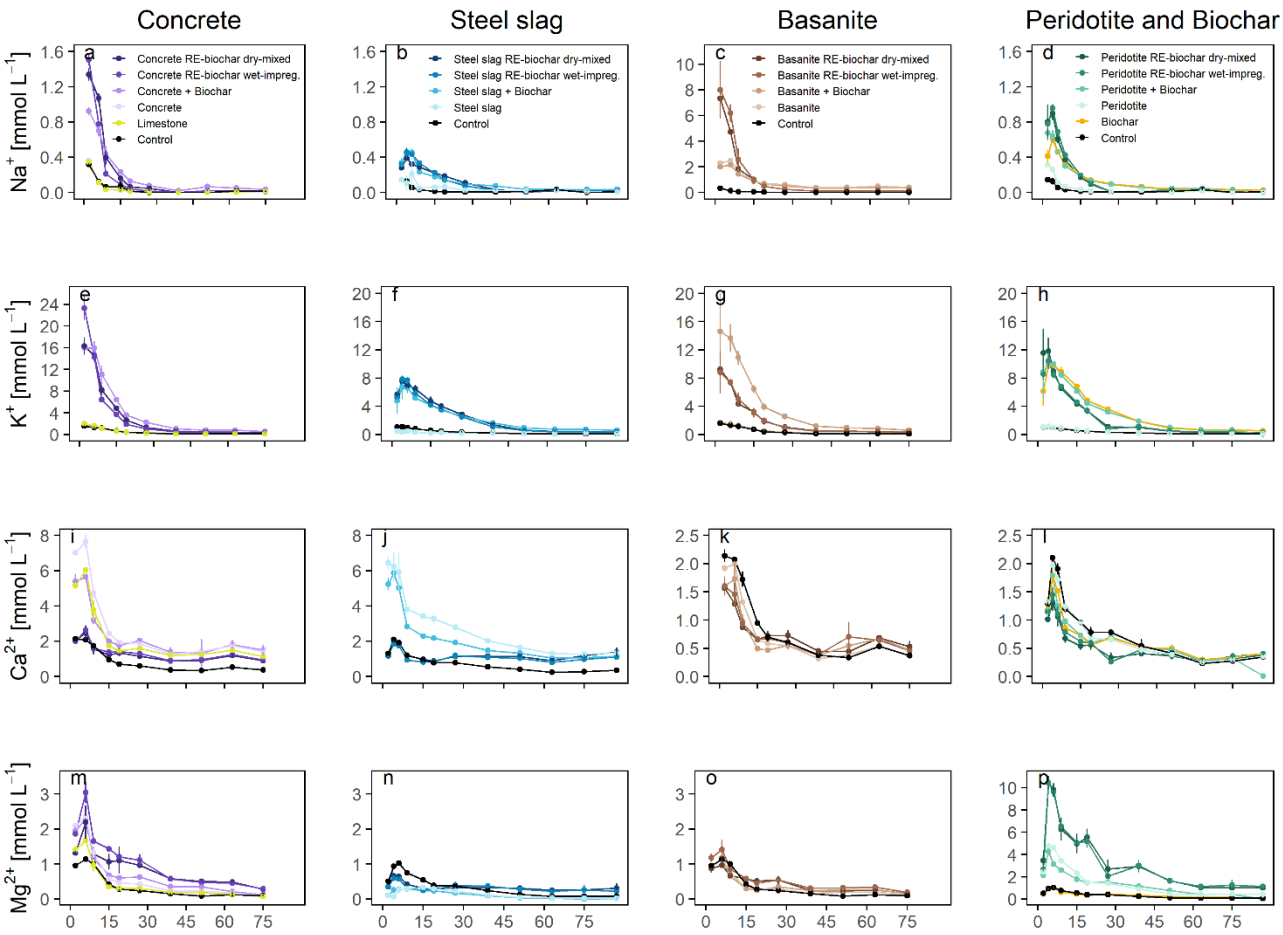

290

291 Figure S8. Time series of major cations a-d) sodium (Na^+), e-h) potassium (K^+), i-l) calcium (Ca^{2+}), and

292 m-p) magnesium (Mg^{2+}). Error bars indicate standard deviations (n=2).

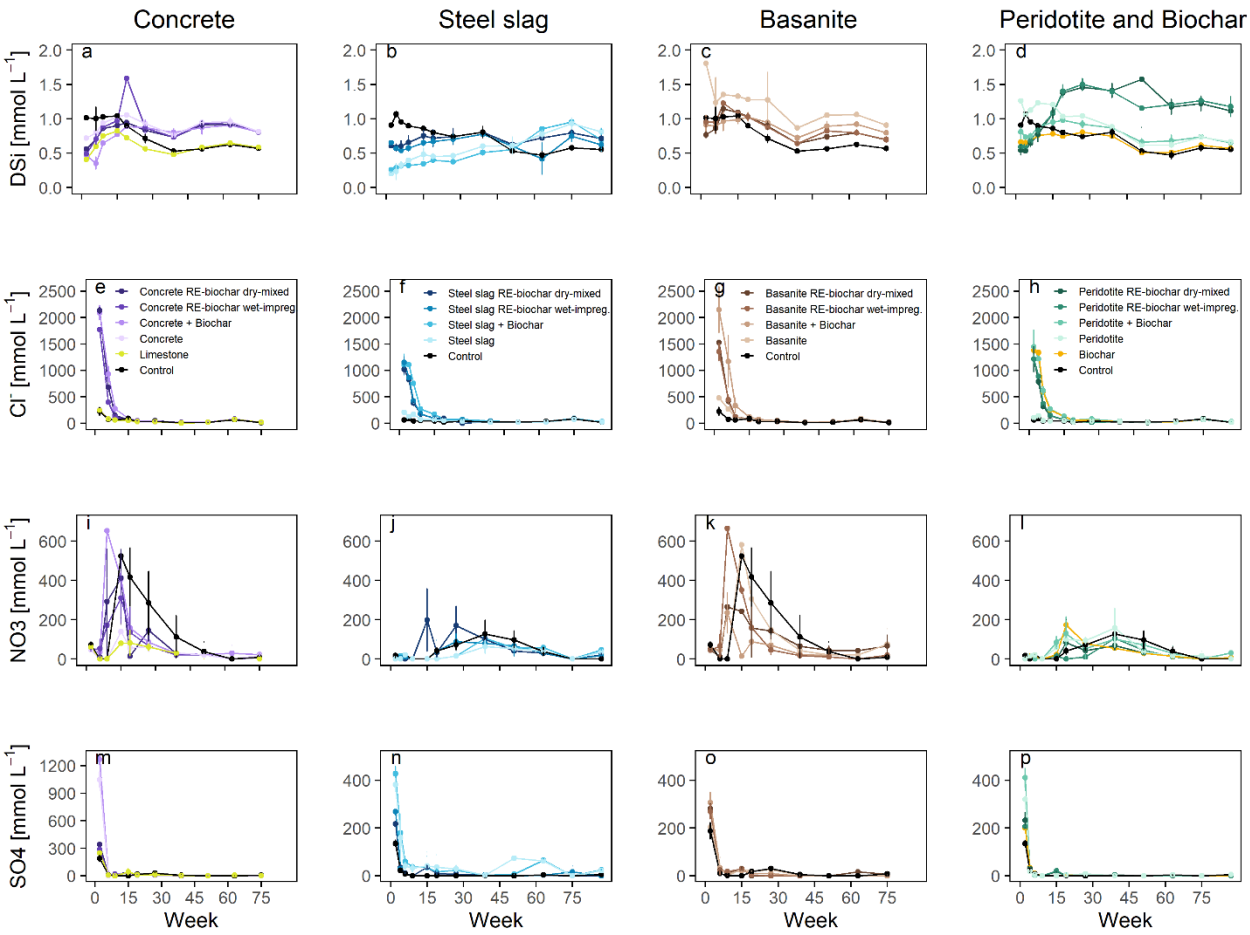

Figure S9. Time series of a-d) dissolved silica (DSi), e-h) chlorine (Cl^-), i-l) nitrate (NO_3^-), and m-p) sulphate (SO_4^-). Error bars indicate standard deviations (n=2).

References

Amann, T., Hartmann, J., Hellmann, R., Pedrosa, E.T., Malik, A., 2022. Enhanced weathering potentials—the role of in situ CO2 and grain size distribution. Front. Clim. 4, 929268. https://doi.org/10.3389/fclim.2022.929268

Ansari, M., Stock, S., Dippold, M.A., Hamburger, S.E., Kammann, C.I., Meyer Zu Drewer, J., Hagemann, N., Eschenbach, A., Becker, J.N., 2026. Biochar dominated the combined effect of silicate rock powder and biochar application on extracellular enzyme kinetics and nutrient dynamics in a sandy soil. Soil and Tillage Research 262, 107234. https://doi.org/10.1016/j.still.2026.107234

Dickson, A.G., 1981. An exact definition of total alkalinity and a procedure for the estimation of alkalinity and total inorganic carbon from titration data. Deep Sea Research Part A. Oceanographic Research Papers 28, 609–623. https://doi.org/10.1016/0198-0149(81)90121-7

Dietzen, C., Rosing, M.T., 2023. Quantification of CO2 uptake by enhanced weathering of silicate minerals applied to acidic soils. International Journal of Greenhouse Gas Control 125, 103872. https://doi.org/10.1016/j.ijggc.2023.103872

Hansen, H.P., Koroleff, F., 1999. Determination of nutrients, in: Methods of Seawater Analysis. John Wiley & Sons, Ltd, pp. 159–228. https://doi.org/10.1002/9783527613984.ch10

Meredith, W., McBeath, A., Ascough, P., Bird, M.I., 2017. Analysis of biochars by hydropyrolysis (HyPy), in: Singh, B., Camps Arbestain, M., Lehmann, J. (Eds.), . CRC Press, Clayton.

Parkhurst, D.L., Appelo, C.A.J., 2013. Description of input and examples for PHREEQC version 3—A computer program for speciation, batch-reaction, one-dimensional transport, and inverse geochemical calculations, in: U.S. Geological Survey Techniques and Methods. U.S. Geological Survey, Denver, p. 497.

Renforth, P., 2019. The negative emission potential of alkaline materials. Nat Commun 10, 1401. https://doi.org/10.1038/s41467-019-09475-5

Rieder, L., Hagens, M., Poetra, R., Vidal, A., Calogiuri, T., Neubeck, A., Singh, A., Corbett, T., Niron, H., Vicca, S., Vlaeminck, S.E., Janssens, Iris, Verdonck, T., Janssens, Ivan, Li, X., Hammes, J.S., Hartmann, J., 2026. Contribution of dissolved organic carbon to total alkalinity in Enhanced Weathering experiments. Applied Geochemistry 198, 106685. https://doi.org/10.1016/j.apgeochem.2026.106685

Schmidt, H.-P., Abiven, S., Hagemann, N., 2022. Permanence of soil applied biochar. An executive summary for Global Biochar Carbon Sink certification. The Biochar Journal 69–74.

Vorrath, M.-E., Amann, T., Meyer zu Drewer, J., Hagemann, N., Aldrich, C., Börker, J., Seedtke, M., Becker, J.N., Hagens, M., Eschenbach, M., Hartmann, J., 2025. Pyrogenic carbon and Carbonating Minerals for Carbon Capture and Storage (PyMiCCS) Part II: Organic and Inorganic Carbon Dioxide Removal in an Oxisol. Frontiers in Climate. https://doi.org/10.3389/fclim.2025.1592454